



**University of  
Zurich**<sup>UZH</sup>

# Assessment of organic carbon stabilisation in tropical soils - Evaluating soil organic carbon quality and distribution under dry-deciduous forest in south-western Karnataka

ESS 511 Master's Thesis

**Author**

Lisa Maria Pirisinu  
16-703-415

**Supervised by**  
Severin-Luca Bellè

**Faculty representative**  
Dr. Samuel Abiven

31.01.2022  
Department of Geography, University of Zurich

**Assessment of organic carbon stabilisation in tropical soils**  
Evaluating soil organic carbon quality and distribution under dry-deciduous  
forest in south-western Karnataka



**Author:**

Lisa Maria Pirisinu  
16 703 415

**Supervisor:**

Severin-Luca Bellè (severin-luca.belle@geo.uzh.ch)

**Faculty representative:**

Prof. Dr. Samuel Abiven (abiven@biotite.ens.fr)

31<sup>st</sup> January 2022  
Department of Geography, University of Zurich  
Master thesis ESS 511

*"General texts continue to imply incorrectly that  
tropical rain forest soils are uniformly dominated by 'red laterites'.  
Tropical forests are, in fact, diverse [...]"*

(Ghazoul and Sheil 2010)

Cover picture: Dry-deciduous forest in Karnataka (India). Photograph by M. Schiedung (2019).

## Acknowledgments

Throughout the writing of this thesis I have received a great deal of support and assistance. Foremost, I would like to express my appreciation and thanks to my supervisors Severin-Luca Bellè (Soil Science and Biogeochemistry, UZH) and Samuel Abiven (ENS, Paris and CEREEP - Ecotron Île de France), who guided me throughout the duration of this project with helpful advice, patience as well as their own professional knowledge and experience. Their encouragement cannot be overestimated. I also wish to thank Marcus Schiedung (Soil Science and Biogeochemistry, UZH) for his valuable support during lab work and assistance with any incurring questions. Further, I would like to extend my sincere thanks to Thomy Keller (Soil Science and Biogeochemistry, UZH) for his efforts and help in the lab and to others in the 2B group for a kind ear and literally opening doors for me. A special thank you also goes out to Nadja-Tamara Studer who proofread my thesis and to Philipp Rüegg, Cristina Haldemann, Jeannine Suremann and other friends and family for moral support and happy distractions.



## Abstract

Tropical forest soils store approximately 500 Pg of carbon and are therefore a crucial component of the global carbon cycle. However, soil organic carbon (SOC) dynamics are severely understudied in the tropics and hence underrepresented in global models. Here, three major soil types (Lixisol, Ferralsol and Vertisol) under tropical, dry deciduous forest from the sub-humid Western Ghats were studied. The soil samples were treated using a combination of particle size and density fractionation, to separate the labile particulate organic matter (POM) fraction from the more stable sand and aggregates (S+A) as well as silt and clay (s+c) fractions. The fractions were analysed using organic carbon analysis (total organic carbon (TOC),  $^{13}\text{C}$ ) as well as mid-infrared spectroscopy. Most SOC was stored in the s+c fraction and the soils' TOC concentrations were mainly influenced by clay content in Lixisols and Ferralsols and the interaction of clay minerals with oxides in Vertisols. Fractions were increasingly enriched in  $\delta^{13}\text{C}$  in the following order:  $\text{POM} < \text{S+A} < \text{s+c}$ , indicating highest SOC stability in the s+c fraction and the importance of tropical soils for carbon storage. This thesis provided valuable data on SOC distribution and quality in tropical soils as well as new insights into the stabilisation mechanisms at play.

# Contents

|          |  |           |
|----------|--|-----------|
| <b>1</b> | <b>Introduction</b>  | <b>1</b>  |
| <b>2</b> | <b>Theoretical background</b>  | <b>3</b>  |
| 2.1      | Soil organic carbon stabilisation . . . . .                                    | 3         |
| 2.2      | Principal soil types . . . . .   | 6         |
| 2.2.1    | Ferralsol . . . . .  | 6         |
| 2.2.2    | Lixisol . . . . .  | 6         |
| 2.2.3    | Vertisol . . . . .   | 6         |
| 2.3      | $\delta^{13}\text{C}$ signal of soil organic carbon . . . . .                  | 7         |
| <b>3</b> | <b>Study site</b>  | <b>8</b>  |
| 3.1      | Geology and soil . . . . .   | 8         |
| 3.2      | Vegetation . . . . .   | 10        |
| 3.3      | Hydrology . . . . .  | 10        |
| <b>4</b> | <b>Methodology</b>   | <b>12</b> |
| 4.1      | Sampling . . . . .   | 13        |
| 4.1.1    | Sampling design . . . . .  | 13        |
| 4.1.2    | Sample preparation . . . . .   | 13        |
| 4.2      | Chemical analysis . . . . .  | 13        |
| 4.2.1    | Fractionation . . . . .  | 13        |
| 4.2.2    | HCl fumigation and combustion . . . . .  | 15        |
| 4.2.3    | Diffuse reflectance mid-infrared Fourier transform spectroscopy . . . . .      | 17        |
| 4.3      | Statistical analysis and data visualisation . . . . .                          | 18        |
| <b>5</b> | <b>Results</b>   | <b>20</b> |
| 5.1      | Difference in carbon content between sampling sites . . . . .                  | 20        |
| 5.1.1    | Overview of total carbon and total organic carbon contents . . . . .           | 20        |
| 5.1.2    | Difference in total organic carbon between sampling sites with depth . . . . . | 21        |
| 5.2      | Total organic carbon and $\delta^{13}\text{C}$ trends with depth . . . . .     | 22        |
| 5.2.1    | Bulk soil . . . . .  | 22        |
| 5.2.2    | Particulate organic matter . . . . .   | 23        |
| 5.2.3    | Sand and aggregates . . . . .  | 23        |
| 5.2.4    | Silt and clay . . . . .  | 24        |
| 5.3      | Diffuse reflectance mid-infrared Fourier transform spectroscopy . . . . .      | 24        |
| 5.3.1    | Bulk soil . . . . .  | 24        |
| 5.3.2    | Particulate organic matter . . . . .   | 27        |
| 5.3.3    | Sand and aggregates . . . . .  | 27        |
| 5.3.4    | Silt and clay . . . . .  | 28        |

|          |   |           |
|----------|---|-----------|
| 5.4      | Ratio of labile to stable compounds . . . . .                                 | 31        |
| <b>6</b> | <b>Discussion</b>   | <b>32</b> |
| 6.1      | General patterns . . . . .  | 32        |
| 6.2      | Differences in soil organic carbon between sampling sites . . . . .           | 33        |
| 6.2.1    | Vertisols . . . . .   | 33        |
| 6.2.2    | Lixisols and Ferralsols . . . . .   | 34        |
| 6.3      | Relative importance of stabilisation mechanisms . . . . .                     | 35        |
| 6.4      | Methodological limitations . . . . .  | 36        |
| <b>7</b> | <b>Conclusion</b>   | <b>38</b> |
| <b>8</b> | <b>Outlook</b>  | <b>39</b> |
|          | <b>Bibliography</b>   | <b>40</b> |
| <b>A</b> | <b>Appendix</b>   | <b>45</b> |
| A.1      | Data overview . . . . .   | 45        |
| A.1.1    | Overview of soil samples and fractionation results . . . . .                  | 45        |
| A.1.2    | Checking peaks in the DRIFT spectra . . . . .                                 | 49        |
| A.2      | Data processing and visualisation with R . . . . .                            | 52        |
| A.2.1    | Statistical testing of total organic carbon . . . . .                         | 52        |
| A.2.2    | Calculating significance levels . . . . .                                     | 54        |
| A.2.3    | Plotting of TOC and $\delta^{13}\text{C}$ . . . . .                           | 56        |
| A.2.4    | DRIFTS: Extraction of integrated band areas and testing the new sample holder | 57        |
| A.2.5    | Testing correlation variables for normality . . . . .                         | 58        |

## List of Figures

|    |  |    |
|----|--|----|
| 1  | Overview of stabilisation mechanisms. . . . .  | 5  |
| 2  | Map of Mule Hole. . . . .  | 8  |
| 3  | Soil profiles at the sampling sites. . . . .   | 9  |
| 4  | Dry-deciduous forest. . . . .  | 10 |
| 5  | Overview of the applied methods. . . . .   | 12 |
| 6  | Sampling design. . . . .   | 13 |
| 7  | The fractionation process. . . . .   | 14 |
| 8  | Photographs of the fractionation process. . . . .  | 15 |
| 9  | Methodical problems of fumigation. . . . .   | 16 |
| 10 | Visualisation of the sample holder used for DRIFTS measurements. . . . .                       | 17 |
| 11 | Distribution of TOC concentration between sampling sites per depth. . . . .                    | 21 |
| 12 | Proportion of each soil fraction to the TOC of the bulk soil, normalised to 100%. . . . .      | 23 |
| 13 | TOC and $\delta^{13}\text{C}$ of the bulk soil and POM fraction. . . . .                       | 25 |
| 13 | TOC and $\delta^{13}\text{C}$ of the S+A and s+c fractions. . . . .                            | 26 |
| 14 | DRIFTS compound ratios of the bulk soil and POM fraction. . . . .                              | 29 |
| 14 | DRIFTS compound ratios of the S+A and s+c fractions. . . . .                                   | 30 |
| 15 | Correlation between DRIFT band ratios and SOC fractions. . . . .                               | 31 |
| 16 | DRIFT spectra of the bulk soil and POM fraction. . . . .                                       | 50 |
| 17 | DRIFT spectra of the S+A and s+c fraction. . . . .   | 51 |
| 18 | QQ-plots of F3 at 30-45 cm and 45-60 cm for the S+A fraction. . . . .                          | 53 |
| 19 | ANOVA residuals. . . . .   | 53 |
| 20 | Histogram of the bulk soil data subset of TOC [g C kg <sup>-1</sup> soil] at 45-60 cm. . . . . | 53 |
| 21 | Code used to calculate significance levels. . . . .  | 54 |
| 21 | Code used to calculate significance levels. . . . .  | 55 |
| 22 | Code used to plot the TOC content and $\delta^{13}\text{C}$ singals. . . . .                   | 56 |
| 24 | QQ-plots of DRIFTS and fractionation correlation . . . . .                                     | 58 |

## List of Tables

|   |   |    |
|---|---|----|
| 1 | Characteristics of the soil types Lixisol, Ferralsol and Vertisol. . . . .                                | 7  |
| 2 | Overview of TC, TOC and $\delta^{13}\text{C}$ for the bulk soil. . . . .                                  | 20 |
| 3 | Overview of correlation tests between slow and fast cycling DRIFT compounds and carbon fractions. . . . . | 31 |
| 4 | Overview of soil samples. . . . .   | 45 |
| 5 | TC, TOC and $\delta^{13}\text{C}$ of the carbon fractions. . . . .  | 48 |
| 6 | Overview of data transformations of TOC. . . . .  | 52 |
| 7 | P-values of the statistical tests applied to the TOC data. . . . .  | 52 |
| 8 | Overview of the non-parametric pairwise comparison of TOC. . . . .  | 53 |

# 1 Introduction

The global carbon cycle is made up of several carbon pools with the soil representing one of the major reservoirs apart from the oceans and sedimentary rock. It contains approximately 2'400 Pg of carbon (up to 2 m depth) and hence stores almost double the amount of carbon than the atmosphere and above ground biomass together (Paustian et al. 2016). Thereby, forest soils constitute 31 % of the total land area, of which tropical forests cover 45 % (FAO 2020), storing over 500 Pg of carbon (Jackson et al. 2017). The soil organic carbon (SOC) pool is sensitive to changes in climate and environment. However, it remains unclear how and on what timescale it will respond to such changes, since soil does not function as one unit. Instead, it combines interactions of solid, liquid, and gaseous phases with biology, over vastly different time spans and spatial scales. Hence soil system's complexity has not been accurately incorporated into models of SOC dynamics, since most studies rely on general assumptions about SOC by climate and soil type (Schmidt et al. 2011). Therefore, uncertainties are large, leading to differences of up to 50 % in estimates of global SOC storage (Kögel-Knabner and Amelung 2021). Moreover, attempts at relating global SOC data to maps, are limited by challenges arising due to different soil reference systems used internationally and dissension in model parametrisation (Kögel-Knabner and Amelung 2021; Schmidt et al. 2011).

Generally, conceptual models suggest that SOC quality, quantity and distribution depend on the source of carbon input, occlusion within aggregates, incorporation in organo-mineral complexes and the location within the soil profile (Schrumpf et al. 2013). These factors in turn vary depending on the heterogeneity of vegetation composition and litter input, on parent material, landscape position, soil type and land use history. Modelling such dynamics requires an underlying understanding of SOC stabilisation and destabilisation processes, as well as sufficient data for the initialisation and validation of SOC models (Sollins et al. 2007; Zimmermann et al. 2007). Hence, studies at a regional, or better landscape level, are crucial to represent the soil's heterogeneity (Bellè et al. 2022). Moreover, the validation of conceptual SOC subunits would increase the confidence in SOC models and enhance the understanding of interactions between SOC and the pedogenic environment (Zimmermann et al. 2007). One approach to define such subunits are SOC fractionation procedures, which have been applied in many studies over the years (Lützwow et al. 2007; Sollins et al. 2007).

Physical fractionation, as a combination of particle size and density fractionation, is a useful tool to study the distribution and quality of SOC in aggregates and in association with minerals (Lützwow et al. 2007; Poeplau et al. 2013; Zimmermann et al. 2007). However, it has rarely been applied to full soil profiles or tropical soils (Toriyama et al. 2015). Kögel-Knabner and Amelung (2021) mention, that research on SOC has so far mostly focused on temperate and man-made soils, leaving others underrepresented (Kögel-Knabner and Amelung 2021). A literature search of tropical soils and fractionation (keywords: "fractionation" OR "fraction\*" AND "soil organic carbon" OR "SOC" AND "tropic\*" OR "subhumid") showed few studies done in tropical climate. Thereof, most analysed cropland and used varying definitions and approaches to fractionation, since SOC fractions have been considered sensitive indicators to changes in agricultural practices (Pulido-Moncada et al. 2018). Moreover, it did not

show any results on fractionation being applied to forest soils that are not currently under cultivation. And to our knowledge, there has so far been no study applying the fractionation method proposed by Zimmermann et al. (2007) and Poeplau et al. (2013) on tropical soils under secondary forest.

The aim of this thesis was to explore the quality of SOC within different carbon fractions along the profile depth of tropical soils of southwestern India (Karnataka). This was done using physical fractionation consisting of dispersion, density and particle size separation based on Zimmermann et al. (2007). The method aims at separating bulk soil into compartments with different physico-chemical properties, which are assumed to exhibit varying sensitivity to disturbance. Further, it relies on the premise that the association of soil particles and aggregates is the key component in SOC stabilisation (Poeplau et al. 2013). The resulting fractions were then analysed for their carbon and  $\delta^{13}\text{C}$  signals using a Picarro dry combustion module with Cavity Ring-Down spectrometer (see section 4.2.2). Secondly, diffuse reflectance mid infrared Fourier transform spectroscopy (DRIFTS) was used to determine the relative abundance of chemical compounds such as aromatic or aliphatic carbon within a sample (see section 4.2.3). This method allowed for a qualitative assessment of carbon dynamics, that is carbon input sources and microbial decomposition (Bellè et al. 2022; Laub et al. 2019). Thereby the research questions leading this thesis were 1) How does the composition of SOC (distribution within fractions) vary between soil types and depth? and 2) How does the distribution of SOC in fractions relate to SOC stability? Hence, the goal was to quantify SOC fraction and distribution of carbon pools at the different sampling sites based on fractionation. Secondly the aim was, to qualitatively describe carbon quality at the different sampling sites based on DRIFTS and Picarro measurements for all fractions, and lastly, to propose driver(s) of differences in SOC quality and distribution between soil types and sampling sites.

## 2 Theoretical background

### 2.1 Soil organic carbon stabilisation

SOC is assimilated through photosynthesis by primary producers and put into the soil via litter, roots, and exudates. Conversely, the output of soil carbon happens via heterotrophic and autotrophic respiration, leaching, combustion, erosion, or the removal of biomass, such as logging (Weil and Brady 2017). The rate of decomposition however, is influenced by various carbon stabilisation mechanisms (e.g. Bruun et al. 2010; Kögel-Knabner and Amelung 2021; Schmidt et al. 2011). The SOC turnover can be altered by different physico-chemical and biological stabilisation mechanisms, which depend on the surrounding environment and the degree of soil development but less on compound chemistry (Kögel-Knabner and Amelung 2021; Schmidt et al. 2011). Factors limiting decomposition and stabilising SOC are firstly, translocation of SOC to deeper soil depth, either via perturbation processes or the advection of soil solution (Buettner et al. 2014; Rumpel and Kögel-Knabner 2011). Secondly, nutrient limitation, energy scarcity, or the fragmentation of microorganism habitat might restrict carbon mineralisation. Especially, in deeper soil horizons, where SOC is distributed more sparsely (Schmidt et al. 2011). Thirdly, SOC can be physically protected through aggregation or adsorption to mineral and oxide surfaces (Bruun et al. 2010; Kögel-Knabner and Amelung 2021; Zimmermann et al. 2007). The relative importance of these mechanisms with respect to increasing SOC persistence, has not been conclusively analysed. However, many studies suggest that clay mineralogy, the association of SOC with oxides as well as aggregate formation are the main drivers of carbon stabilisation in soil (Bruun et al. 2010; Buettner et al. 2014; Kögel-Knabner and Amelung 2021; Pulido-Moncada et al. 2018).

Initial decomposition rates of SOC correlate with its chemical composition, yet thermodynamically unstable SOC has been shown to persist for millennia (Schmidt et al. 2011). Hence, Kögel-Knabner and Amelung (2021) suggest that the co-precipitation of SOC with iron- (Fe) and aluminium- (Al) oxides, as well as the association with oxides, carbonates and soil biota (for example microbial cells and root exudates) lead to its occlusion within aggregates (Kögel-Knabner and Amelung 2021). These might be structured hierarchically, whereby organic molecules bound to the mineral fraction compose micro-structures, which are further collocated to macroaggregates through microbial macromolecules, root and hyphae fragments (Cates et al. 2022) (see Figure 1). This has been described for multiple soil types such as Luvisols and Vertisols (Kögel-Knabner and Amelung 2021). Additionally, Six et al. (2000) found that soils with 2:1 clay mineralogy had higher carbon contents in macroaggregates compared to microaggregates. This was however not case for soils with mixed mineralogy (Six et al. 2000). Further this process seems less prominent in highly weathered soils like as Ferralsols, where adsorption to Fe-oxides appears to be dominant (Kögel-Knabner and Amelung 2021).

The extent to which SOC (in the form of organic matter) is stabilised, is controlled by the specific surface area of fine-sized minerals. These vary with soil type and include layered clay minerals and Fe- and Al-oxides which then form organo-mineral compounds (Blume et al. 2016; Kögel-Knabner and Amelung 2021). Since oxides have low solubility at common pH levels, they accumulate during weathering and soil formation. While Fe oxidises and precipitates as oxide mineral,  $\text{Al}^{3+}$  usually forms



aluminosilicate clays (Blume et al. 2016). Additionally, the reactivity of these minerals differs with soil pH, base saturation and organic matter chemistry (Kögel-Knabner and Amelung 2021). The formation of inner-sphere complexes through ligand-exchange plays an important role for SOC stabilisation in acidic soils. Here Al- and Fe-oxides, as well as the edge surfaces of clay minerals offer high specific surface areas for this type of interactions. Conversely, the ionic bond between organic cations and negatively charged clay minerals becomes more relevant at higher pH. Further, polyvalent cations such as  $\text{Ca}^{2+}$  or  $\text{Al}^{3+}$  can increase the sorption of organic acids to clays with exchangeable cations, such as smectite (see Figure 1). In the case of neutral minerals surfaces such as kaolinite, Van der Waals interactions bind larger molecules (Blume et al. 2016).

Phyllosilicate clays provide surfaces for the sorption of SOC. Hereby, it is generally accepted that the stabilisation capacity of clay minerals decreases as follows: allophane > smectite > illite > kaolinite (Bruun et al. 2010). Thereof, smectite and kaolinite are the predominant clay types found in the tropics. While smectite is assumed to have a high capacity to store SOC through cation bridges, kaolinitic clays are regarded as unreactive due to their 1:1 layer structure. Kaolinites have little or no permanent charge and very little isomorphic substitution, which leads to low cation exchange capacities and surface areas (Schulze 2005). In contrast, the 2:1 layer structure of smectite allows for exchangeable cations in the interlayer and hence provides a high surface area and adsorptive capacity (Schulze 2005). This also leads to a shrink–swell behavior, which is most commonly found in Vertisols (section 2.2.3). However, Bruun et al. (2010) stated, that kaolinite might stabilise SOC to a similar degree than smectite and the content of Fe- as well as Al- oxides might modify its stabilisation capacity (Bruun et al. 2010). This is confirmed by Kögel-Knabner and Amelung (2021), who note that some studies have found no significant difference in mean residence time between kaolinite-bound and smectite-bound SOC in different soils. They conclude that the charge and the amount of available mineral surface was decisive for SOC stabilisation (Kögel-Knabner and Amelung 2021).

Studies have found that redox potential is an important predictor of SOC stabilisation, since Fe(III)-oxides readily dissolve under reducing conditions (Blume et al. 2016). As an example, Bruun et al. (2010) found that free Fe- and Al-(hydr-)oxides stabilised significant amounts of SOC and Kaiser and Guggenberger (2000) provided evidence, that hydrous metaloxides are the most important sorbents for dissolved organic carbon (DOC). Conversely, Chen et al. (2020) emphasise that Fe does not intrinsically protect SOC from decomposition. Rather, it may serve as a connective agent for aggregation and as sorbent under oxic conditions but also enables dispersion of aggregates in an anoxic environment (Chen et al. 2020; Scheinost 2005). Similarly, Buettner et al. (2014) observed that Fe-reducing conditions released high concentrations of carbon because of the dissolution of Fe-oxide coatings binding colloids into larger aggregates. This could cause the mobilisation and migration of SOC from the surface to the subsoil (Buettner et al. 2014).

The transport of mobilised carbon to deeper soil depths increases SOC stability. This can be attributed to lower microbial activity with depth, and a lack of other sources for microbial growth, such as nitrogen or phosphorous (Kögel-Knabner and Amelung 2021). Additionally, SOC might be spatially

isolated due to the low SOC concentration at depth and therefore not accessible to microorganisms and extracellular enzyme activity (Rumpel and Kögel-Knabner 2011; Schmidt et al. 2011). Schmidt et al. (2011) report, that subsoils contribute more than half of the global soil carbon stocks and Kögel-Knabner and Amelung (2021) state that 47 % of the top meter's SOC stocks is found within 30-100 cm depth (Kögel-Knabner and Amelung 2021). Hence, vertical translocation of SOC might significantly reduce mineralisation (Buettner et al. 2014). However, reliable and agreeing data on these processes is missing (Kögel-Knabner and Amelung 2021).

SOC transport to the subsoil can be mediated through percolation of dissolved organic carbon (DOC) but also via perturbation processes and will vary depending on soil type and topographic position (Kögel-Knabner and Amelung 2021; Schmidt et al. 2011). DOC will flow downwards along preferential flow pathways, of which some might be lost to leaching and other parts will be adsorbed or precipitated along with Fe- and Al-oxides (Rumpel and Kögel-Knabner 2011). However, the weathering of the soil's parent material decreases with depth and so does the mineral's reactivity and stabilisation capacity (Kögel-Knabner and Amelung 2021). Further, particulate organic matter (POM) can be transported by perturbation and falling into cracks in the soil (Buettner et al. 2014). Additionally, the swelling and shrinking of Vertisols, leads to self-ploughing, that is peloturbation, and an increase in SOC of the subsoil (Kögel-Knabner and Amelung 2021). So does bioturbation, which in case of tropical soils is mostly facilitated by termites and rain worms (Ghazoul and Sheil 2010).

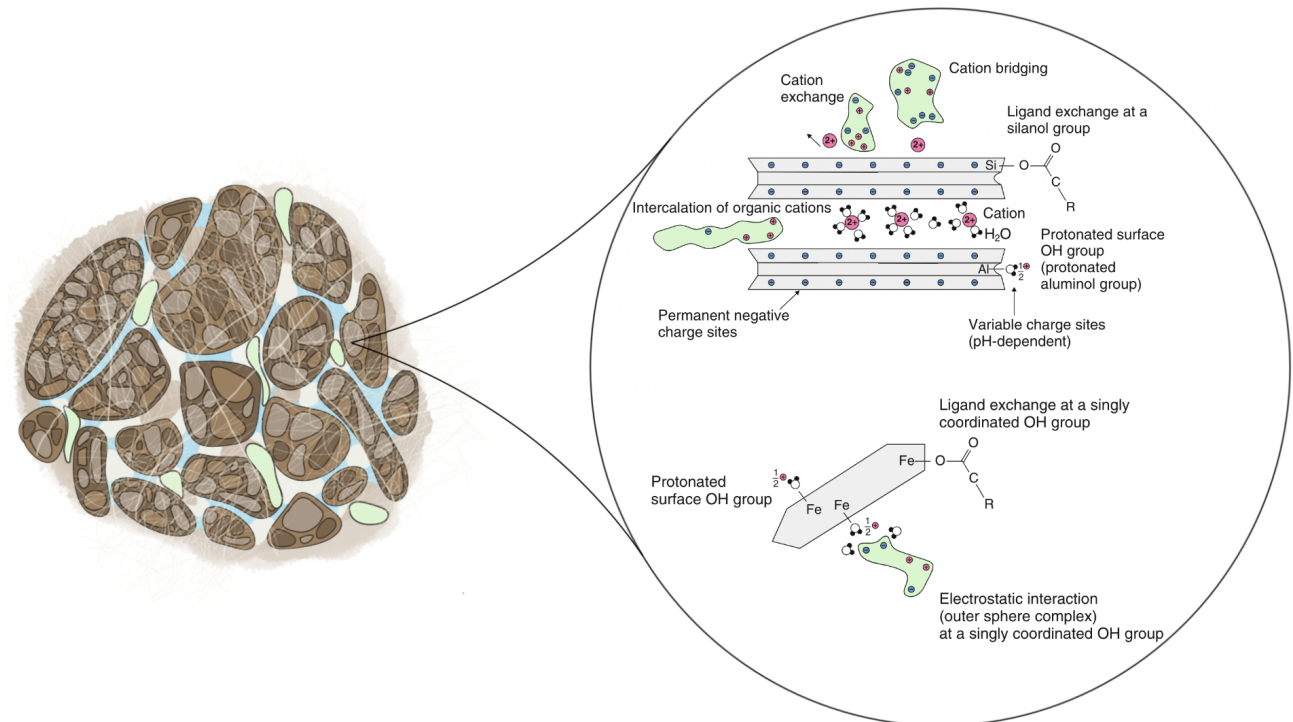


**Figure 1:** Aggregates can be structured hierarchically. Thereby roots, hyphae and exudates (thin, white lines) act as glue, holding together organic matter (light green) and smaller aggregates. On a smaller scale, SOC in the form of organic matter is stabilised by phyllosilicates (top right) and (hydr-)oxides (bottom right), which act as cementing agents. In blue and white are pore spaces filled with water and air respectively (based on and adapted from Blume et al. 2016; Costa et al. 2018).

## 2.2 Principal soil types

Tropical soils such as Ferralsols and Lixisols are underrepresented in SOC studies (Kögel-Knabner and Amelung 2021), especially under tropical forest. Despite making up 45 % of the global forested land area (FAO 2020), only 11 % of all soil profiles in the World Soil Information Service database are soils from tropical or subtropical forests (Bellè et al. 2022). The main reasons being inaccessibility of study sites, lack of infrastructure and financial resources at sites of interest as well as missing methodology, developed for tropical soils. Additionally, tropical forest soils are often thought to be dominated by red, deeply weathered soils, when they are in fact highly diverse (Ghazoul and Sheil 2010). They differ depending on soil forming factor such as their parent material, topography and degree of weathering (Kögel-Knabner and Amelung 2021). The three soil types covered in this thesis are Ferralsols, Lixisols and Vertisols, which cover 19.3 %, 11.2 % and 8.6 % of the global forested land surface respectively (Bellè et al. 2022).

### 2.2.1 Ferralsol

Kögel-Knabner and Amelung (2021) write, that the Ferralsols are red (hematite) or yellow (goethite) soils which are primarily found in the humid tropics. Due to high temperatures and precipitation, they are deeply weathered. Hence, the mineral assemblage consists of secondary minerals, such as low activity clay (mainly kaolinites) and high contents of Fe- and Al-oxides as well as coarse quartz grains. The former indicate the diagnostic ferralic horizon of Ferralsols (see Table 1). Further, Ferralsols are deeply rooted and therefore experience SOC input to several meters and hence profit from multiple stabilisation mechanisms. Although it is often assumed, that Ferralsols are stabilised by inorganic components (oxides), it has been shown, that binding of organic compounds at mineral surfaces is a crucial process, leading to the accrual of SOC by means of organo-mineral associations (Kögel-Knabner and Amelung 2021).

### 2.2.2 Lixisol

The World Reference Base for Soil Resources classifies Lixisols as soils with an accumulation of low activity clays in an argic B horizon and high base status (see Table 1) (IUSS Working Group WRB 2015). Thereby, the main pedogenic process is the dispersion, transport and accumulation of clay from the E to the B horizon. This type of soil is deeply weathered, and the clay fraction consists mainly of kaolinite and few Fe-oxides. They are known to store comparatively little SOC and are prone to erosion. Lastly, they are generally found in old landscapes with undulating topography under forests in humid tropical climate (Kögel-Knabner and Amelung 2021).

### 2.2.3 Vertisol

Vertisol are mainly found in lower landscapes such as valley bottoms or river basins that are periodically wet (Barbiéro et al. 2010) as well as over clay rich sediments or mafic rock (Kögel-Knabner and Amelung 2021). Further, they frequently occur in semi-arid to sub-humid climates with distinct wet and dry

seasons. Moreover, Vertisols form a landscape with micro high and lows (Kögel-Knabner and Amelung 2021). Thereby, highs usually dry out faster and are prone to accumulating calcium carbonates, while the lows are moister and richer in SOC and pedogenic oxides (Kögel-Knabner and Amelung 2021; Pal 2019). Additionally, Vertisols contain high amounts of smectites, which lead to swelling and shrinking of the soils. The result is an uneven uplift of the soil and mixing of the profile (peloturbation) with creation of wedge-shaped aggregates, which are diagnostic for the vertic horizon (Kögel-Knabner and Amelung 2021). However, the high smectite content also leads to a strong buffering capacity and supports high base saturation and a high pH. Under decreasing pH, smectite is hydrolysed to kaolinite (Kögel-Knabner and Amelung 2021).

**Table 1:** Characteristics of the soil types Lixisol, Ferralsol and Vertisol. CEC = cation exchange capacity, BS = base saturation. (adapted from Kögel-Knabner and Amelung 2021)

| Soil type<br>+ Horizons | Diganostic<br>horizon        | Texture  | Mineral<br>components                                     | pH  | Physical properties   |
|-------------------------|------------------------------|--|---|-----|---|
| Lixisols<br>A-E-Bt-C    | Argic;<br>lowCEC;<br>high BS | Silty (topsoil);<br>loamy or clayey<br>(subsoil) | 1:1 clay minerals<br>(Kaolinite)                          | 5-6 | Subangular,<br>blocky structure   |
| Ferralsols<br>A-Bo-C    | Ferralic                     | Clayey   | 1:1 clay minerals<br>(Kaolinite)                          | 5   | Well-drained, depp solum;<br>weak macrostructure,<br>strong microstructure      |
| Vertisols<br>A-Bi-C     | Vertic                       | Clayey   | 2:1 clay minerals<br>(1:1 clay minerals);<br>>= 30 % clay | 6-8 | Cracks;<br>hard when dry, sticky when wet;<br>wedge-shaped aggregates (subsoil) |

### 2.3 $\delta^{13}\text{C}$ signal of soil organic carbon

The ratio of the stable  $\delta^{13}\text{C}$  isotope of SOC and  $\text{CO}_2$  generally increases with depth (Rumpel and Kögel-Knabner 2011). This trend can on one hand be attributed to the stabilisation of SOC after passing microbial utilization cycles, leading to heavier  $\delta^{13}\text{C}$  in the remaining SOC. This is due to the preferential decomposition of light  $^{12}\text{C}$  to  $\text{CO}_2$ , leaving heavier  $^{13}\text{C}$  in SOC, and an increasing contribution of microbial carbon. On the other hand, preferential stabilisation of substrates with light or heavy  $\delta^{13}\text{C}$  can lead to difference in  $^{13}\text{C}/^{12}\text{C}$  composition (Gunina and Kuzyakov 2014; Rumpel and Kögel-Knabner 2011): For example the chemical sorption of  $\delta^{13}\text{C}$  enriched compounds like cellulose, over depleted compounds such as lignin (Rumpel and Kögel-Knabner 2011). Such processes disconnect them from steps of carbon utilisation by microorganisms and lead to different  $^{13}\text{C}/^{12}\text{C}$  signatures in various SOC fractions (Gunina and Kuzyakov 2014). Conversely, a decrease of  $\delta^{13}\text{C}$  has been observed under C4 grassland vegetation where fires are frequent, leading to input of  $\delta^{13}\text{C}$  depleted, charred material (Rumpel and Kögel-Knabner 2011). Additionally, it is important to keep in mind that the isotopic signal in C4 vegetation ranges between -17 and -9‰, while that for C3 vegetation lies between -40 and -20‰ (Staddon 2004).

### 3 Study site

The experimental watershed of Mule Hole covers an area of 4.1 km<sup>2</sup> and is located at 11°44' N and 76°27' E in Karnataka (Chamrajnagar District) (Barbiéro et al. 2010). It is part of the Cauvery Basin on the Deccan Plateau and is situated in Western Ghats' rain shadow (Bellè et al. 2022; Riotte et al. 2018) (see Figure 2). More specifically, it lies within the sub-humid transition zone between the semi-arid climate in the east and the humid ridge of the Western Ghats in the west (Riotte et al. 2021), at an elevation of 800-910 m above sea level (Barbiéro et al. 2010). The mean precipitation is 1170 ± 260 mm year<sup>-1</sup> (2003-2019) with approximately 90% of the rainfall originating from the South-West monsoon between June and September, followed by a dry spell and a second, shorter monsoon season. The mean temperature lies at 22 °C (Riotte et al. 2014, 2021).

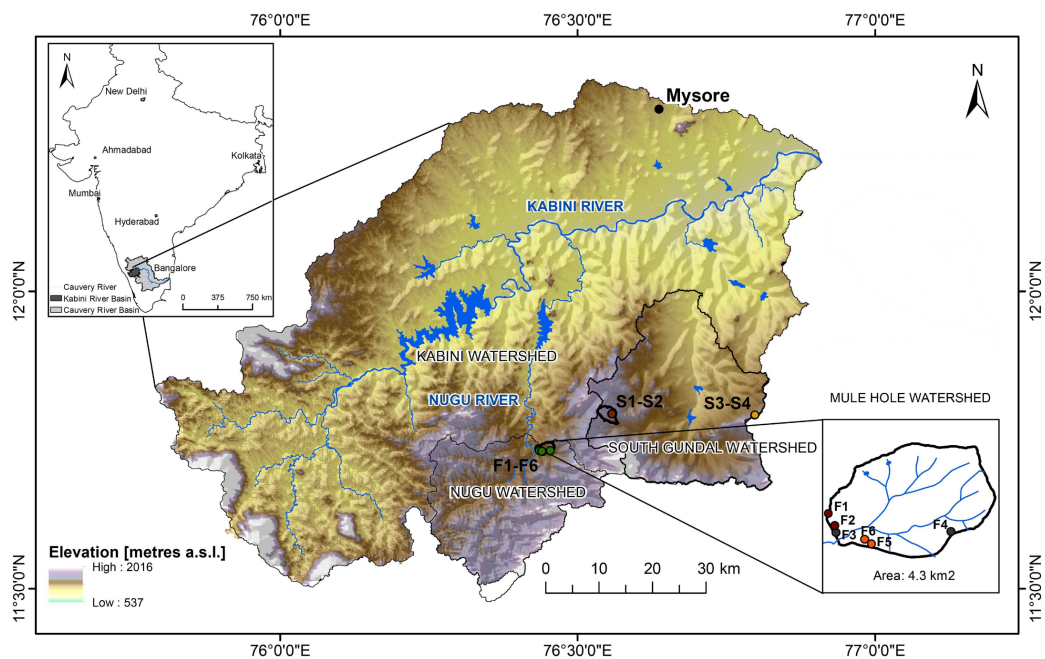


**Figure 2:** Map of the sampling sites at Mule Hole and its geographical location within the Cauvery and Kabini river basins (top left inset). Within the Mule Hole catchment (bottom right inset), the Lixisols are marked in red, Ferralsols in orange and Vertisols in and grey (adapted from Bellè et al. 2022).

#### 3.1 Geology and soil

The Mule Hole catchment developed on precambrian gneiss and scattered mafic rocks, mostly amphibolite. They are covered by approximately 15 m of immature saprolite and up to 2 m thick soils (Riotte et al. 2018, 2021). The saprolite's mineralogy consists of "residual quartz, [...] secondary clays (goethite) and clay minerals" (Riotte et al. 2014, p. 118). Further, the soil cover is dominated by (shallow) Ferralsols and Lixisols on the hillslopes as well as Vertisols in the valleys and footslopes (Bellè et al. 2022). The red soils such as Ferralsols and Lixisols developed on gneiss and are the most abundant soil type at the site (66%). The Vertisols are situated on the lower part of the hillslopes and valley bottoms, cover approximately 12% of the watershed area and measure 2 m in depth on



average. Additionally, thicker Vertisols developed on amphibolite in the depressions on the crest line. They contain both kaolinite and smectite as well as Fe-oxyhydroxides. Lastly, the shallow Ferralsols are 1-2 m deep and dominate on the hillslopes (22 %) with secondary minerals comprising of kaolinite and goethite (Riotte et al. 2014, 2018).



(a) F1 xanthic ferralic Lixisol.



(b) F2 ferric Lixisol.



(c) F3 pellic calcic Vertisol.



(d) F4 pellic Vertisol ferric.



(e) F5 lixic Ferralsol.



(f) F6 lixic Ferralsol.

**Figure 3:** Soil profiles at the sampling sites F1-F6. Photographs by M. Schiedung (2019).



The black soils at Mule Hole developed both on amphibolite as well as gneiss saprolite and lie predominantly at the bottom of the valley and along crest depressions. Their thickness ranges from about 2 m at the perimeter to 6 m at the center of the valley and between 0.2-0.5 m at higher levels (Barbiéro et al. 2007). Further, these soils are characterised by a relatively high proportion of smectite clay minerals. These favor shrinking and swelling of the soils, depending on the water content and cause cracks of up to 1.5 m during the dry season (Barbiéro et al. 2010). Subsequently, polyhedric aggregates from the surface may fall into these crevices and prismatic aggregates in the subsoil can be overturned in the process of swelling. Hence, Vertisols are constantly mixed, leading to a deep A horizon and high cation exchange capacity (CEC) in the profile (Stahr et al. 2016).

### 3.2 Vegetation

The Mule Hole catchment is characterised by gentle slopes and a secondary, dry deciduous forest cover, which established prior to India’s independence in 1947 and after its use as teak plantation (Bellè et al. 2022). Different vegetation types have been described, which depend on the underlying geology and landscape position (Barbiéro et al. 2007). Approximately 70% of the watershed area is covered by the ATT facies composed of *Anogeissus latifolia*, *Tectona grandis* and *Terminalia crenulata* as primary tree species and *Themeda trianda* (Elephant grass) as principal understory vegetation (Riotte et al. 2014). Another important vegetation type is the Shorea facies, which comprises of *Shorea roburghii* and *Lagerstroemia microcarpa* (Barbiéro et al. 2007). Additionally, *Lantana camara* has become a dominant and invasive understory plant in recent years (Bellè et al. 2022). The ATT facies can be found at all six of the sampling sites, together with *L. camara* and *T. trianda*. Further, the Shorea facies is only present at F5 (lixic Ferralsol), together with ATT, *L. camara* and *T. trianda* (Bellè et al. 2022). Further, litter fall usually occurs shortly after the monsoon, from December to February, and new leaves grow back before the start of the new rainy season (Riotte et al. 2014, 2018) Lastly, litter composition for the dominant ATT facies is derived mainly from leaves and grass (4380 kg ha<sup>-1</sup> dry mass) with a smaller input of woody material (Riotte et al. 2014).



**Figure 4:** Dry deciduous forest at sampling site F2 with ATT facies. Photograph by M. Schiedung (2019).

### 3.3 Hydrology

The climate at Mule Hole is characterised by irregular but recurring droughts. Moreover, streams in the watershed are temporary and flow for a few hours to days after storm events, during the rainy season (Barbiéro et al. 2007). Hereby, the streams follow the edge of thick Vertisol at the valley

bottoms, meandering through thin patches (Barbiéro et al. 2007; Riotte et al. 2014). Although soils are saturated towards the end of the rainy season (Riotte et al. 2018), the water balance shows that the forest limits groundwater recharge and runoff (Riotte et al. 2014). Thereby, the groundwater levels close to the streams experience much stronger daily to seasonal variation, while the changes are more buffered on hill slopes and at the hill top (Riotte et al. 2021).



## 4 Methodology

The samples used for this thesis were collected by Severin-Luca Bellè (UZH), Marcus Schiedung (UZH), Benjamin Baud (Indo-French Cell for Water Science) and Indian collaborators at the Mule Hole watershed in Karnataka, southern India, in 2019. The watershed is part of the Critical Zone Observatory “Experimental Tropical Watersheds” (CZO BVET) from the M-TROPICS (Multiscale Tropical Catchments) initiative and as such has been widely studied over the past decades (Riotte et al. 2021). The Mule Hole catchment covers an area of 4.1 km<sup>2</sup> and is located in the Bandipur National Park, a strongly protected zone of the Nilgiri Biosphere Reserve (Riotte et al. 2021).

The 72 soil samples used in this thesis encompassed soil depths up to 60 cm and three different soil types. In order to explore the soil’s carbon distribution and quality, the following methods were applied (see Figure 5):

- Fractionation: Allows to separate different SOC functional groups based on particle size as well as density and serves as a preparatory step for further chemical analysis (Poepflau et al. 2013; Zimmermann et al. 2007).
- HCl fumigation and combustion: Acid fumigation removes inorganic carbon from the sample for total organic carbon (TOC) measurement (Walthert et al. 2010). Further, combustion with the Picarro combustion module measures the carbon content and  $\delta^{13}\text{C}$  signal in the sample by means of laser absorption spectroscopy.
- DRIFTS: Diffuse reflectance mid-infrared Fourier transform spectroscopy (DRIFTS) measures the absorbance of mid-infrared light by molecular bonds in a sample. Wavelength-specific peaks can be used as proxy of carbon quality (Laub et al. 2020).

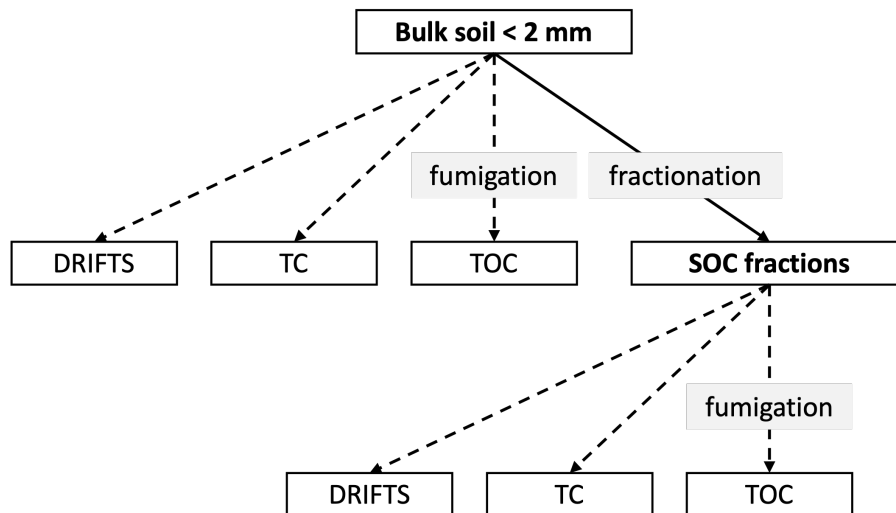


**Figure 5:** Overview of the methods used on the soil samples. The methods were applied to the bulk soil <2 mm as well as all fractions.

## 4.1 Sampling

### 4.1.1 Sampling design

The sampling locations used in this thesis were originally selected for research conducted by S.-L. Bellè and M. Schiedung (UZH). However, they were chosen as sub-samples from a larger set of sampling sites. All sites are covered with dry deciduous forest, lie within a few kilometers of each other and share the same climatic parameters (see Figure 2). Additionally, sites were selected such that they would compose three pairs of sampling sites, where each pair would share the same soil type. Hence two Lixisol (F1, F2), two Vertisol (F3, F4) and two Ferralsol (F5, F6) were chosen. The sampling sites and numbering correspond to the locations and denominations used by Bellè et al. (2022).

The samples were collected from six plots, measuring 25x25 m each and divided into five sampling points, illustrated in Figure 6. Each point was sampled at four depth increments: 0-15, 15-30, 30-45 and 45-60 cm by means of a soil corer. Of the five field replicates, sampling points 1, 3 and 5 were chosen. This amounts to a total of 72 samples analysed in the scope of this thesis: 6 plots à 3 replicates at 4 depth intervals. For each sample, the bulk soil and fractions were analysed separately for organic carbon (section 4.2.1) and DRIFTS measurements (section 4.2.3).

### 4.1.2 Sample preparation

Each sample consisted of a composite of three cores, which were combined in the field. Subsequently, the soil was sieved to <8 mm for homogenisation and air dried. After, the soil was stored in plastic bags for shipment to Switzerland and further processing. Samples were subsequently dried at 40 °C for 48 hours and sieved, in order to extract the <2 mm fraction (Bellè et al. 2022), which is considered to represent the bulk soil (Riotte et al. 2018). This was then archived in plastic bags in dark and dry conditions until further use.

## 4.2 Chemical analysis

### 4.2.1 Fractionation

Different mechanisms are hypothesised to stabilise SOC to varying degrees. Hence multiple conceptual and numerical models have been developed, to better understand and calculate specific turnover times as well as estimate SOC quality and distribution in different soil types (Schmidt et al. 2011). These models define carbon fractions or carbon pools with the goal of distinguishing pools with different turnover times and stabilisation processes. Generally, two labile, two stable and one inert pool are

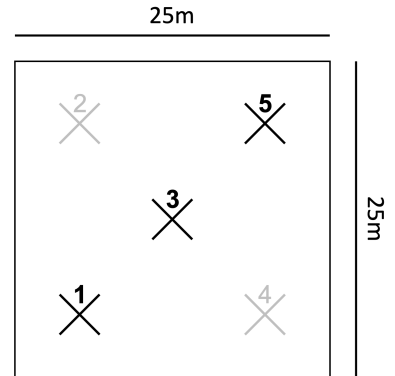


**Figure 6:** Each sampling site contains five pits from which soil samples were taken by soil corer at four depth increments. For the thesis, samples from points 1, 3 and 5 were chosen.

defined (although for this thesis, the inert pool was not separately analysed, but included in the stable fractions) (Zimmermann et al. 2007). One broad approach of pool separation is fractionation based on differences in aggregate or particle size, density or solubility, among others (Lützow et al. 2007). Ideally, these fractions would represent non-composite SOC pool, which are functionally different from each other and decompose homogeneously within the pool (Lützow et al. 2007).

In the context of this thesis, the approach suggested by Zimmermann et al. (2007) and Poeplau et al. (2013) was used to extract the sand and aggregate (S+A), silt and clay (s+c), particulate organic matter (POM) as well as the dissolved organic carbon (DOC) fractions (see Figure 7). The s+c and residual SOC (rSOC) were not distinguished further and are hence forth referred to as s+c. The analysed pools have been proven useful to describe the different decomposition rates and stabilisation mechanisms of SOC (Zimmermann et al. 2007). Hence, s+c and S+A are defined as more stable fractions, while POM and DOC are used as proxies for more labile or dynamic SOC, since they are not physically or chemically stabilised.

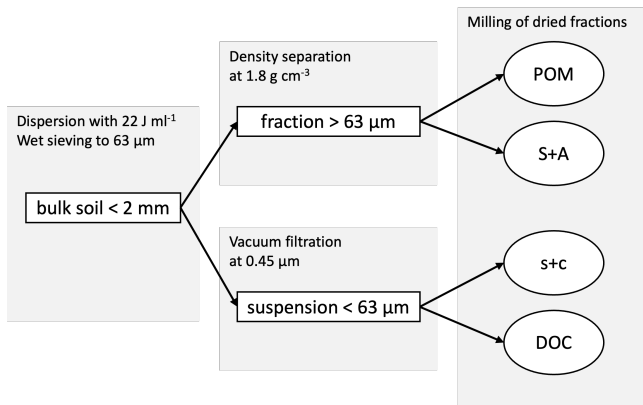


**Figure 7:** Fractionation process and resulting fractions. The fractions consist of particulate organic matter (POM), sand and aggregates (S+A) as well as silt and clay (s+c) and dissolved organic carbon (DOC) (adapted from Zimmermann et al. 2007).

The fractionation process combines particle size and density fractionation and is depicted in Figure 7. In a first step, 20 g of dried bulk soil (<2 mm) were added to a round flask with 150 ml of deionised water and dispersed with an ultrasonic probe at 22 Jml<sup>-1</sup>, with an amplitude of 0.7 and a pulse of 0.5 for 90 seconds. These parameters needed to be adjusted since too much energy could disperse stable aggregates or break down intact organic or mineral particles (Lützow et al. 2007). The correct settings were calculated based on the ratio of the total energy input (based on the total volume of the probe (soil plus water) and the output energy (22 Jml<sup>-1</sup>) defined by Zimmermann et al. 2007) and the energy input per time (based on measurements of temperature

over time). Thereby, the break down of aggregates within the sample could be attributed to stress from cavitation of the fluid during the ultrasonic treatment (Poeplau et al. 2013).

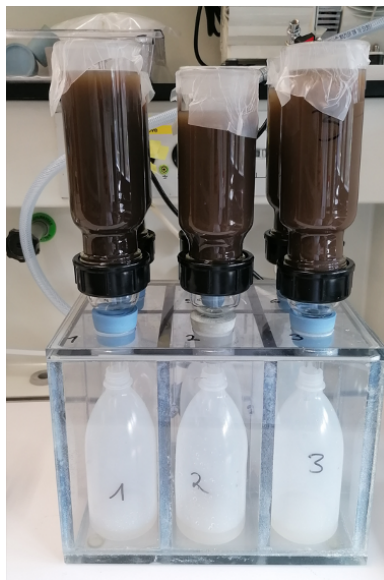
In the next step, the suspension was sieved through a 63 μm sieve, using deionised water and a pressure sprayer (see Figure 8a). This left the S+A and POM fractions (> 63 μm) in the sieve, which were then dried (40 °C) and weighed (Zimmermann et al. 2007). Further, the s+c and DOC suspension was filtered using a vacuum filtration aperture and glass-fiber filters, which retained particles > 0.45 μm (see Figure 8b). Thereby, DOC was collected and an aliquot frozen. Moreover, the s+c fraction was removed from the filter, dried at 40 °C and weighed. In order to separate S+A and POM, the sample was transferred to a centrifuge tube and mixed with 50 ml of sodium polytungstate (SPT)

solution with a density of  $1.8 \text{ gcm}^{-3}$  (Figure 8c). After shaking, the sample was allowed to settle for a minimum of one hour and then centrifuged at 1000 g for 15 minutes. Then, the light fraction (POM) was decanted into a nylon mesh bag and both fractions were thoroughly washed with deionised water to remove all SPT from the sample, before being dried ( $40^\circ\text{C}$ ) and weighed (Zimmermann et al. 2007). Additionally, all dry fractions and the bulk soil were milled to decrease heterogeneity (Walther et al. 2010). POM was milled by hand with an agate pistil and mortar due to the small quantities contained in the samples, while the bulk soil, S+A and s+c were milled with a mixer mill (Retsch MM400) at 30 Hz for 5, 1 minute and 30 seconds respectively. These dried and milled samples were then stored in glass vials until further analysis.

The DOC as well as the rSOC fractions were not further analysed for this thesis. DOC is known to only contribute a little percentage to TOC and results vary, depending on the amount of water used for wet sieving (Poeplau et al. 2013). Additionally, DOC is highly variable in the tropics, depending on the season (Riotte et al. 2018). Therefore, multiple samples over a time span of rainy and dry seasons would have had to be analysed, in order to produce representative results. Hence, the aliquots were not further analysed. Moreover, rSOC would be isolated from the s+c fraction, according to Zimmermann et al. (2007). However, the focus of the thesis did not lie on very stable or inert carbon pools (such as for example pyrogenic carbon) and rSOC was therefore not further distinguished.



(a) Wet sieving



(b) Vacuum filtration



(c) Density fractionation

**Figure 8:** Photographs of the fractionation process.

#### 4.2.2 HCl fumigation and combustion

To determine the carbon content as well as the  $\delta^{13}\text{C}$  signature in the bulk soil and fractions, all samples were combusted using a Picarro Combustion Module Cavity Ring-Down Spectroscopy (CM-CRDS) system. To ensure that samples were measured correctly and to correct any drift from the

instrument, a standard was inserted after every sixth sample, whose carbon content and isotopic ratio were known. The standards were *Miscanthus* for the POM fraction and Chernozem for the bulk soil, S+A and s+c fraction. A maximum of 50 samples at a time were loaded into the auto-sampler connected the combustion module. After starting the measurement, each sample was combusted at 950-1300 °C with O<sub>2</sub> excess and N<sub>2</sub> as carrier gas. Thereby, the carbon was oxidised to CO<sub>2</sub>, that is to <sup>12</sup>CO<sub>2</sub> and <sup>13</sup>CO<sub>2</sub>. The released CO<sub>2</sub> gas pulse then traveled from the reactor to the analyser where the system calculated the isotopic carbon ratio following the  $\delta^{13}$  notation in relation to the Vienna Pee Dee Belemnite (VPDB) standard:

$$\delta = (R_{sample} - R_{standard}) / R_{standard} * 1000\text{‰}$$

where  $R = {}^{13}\text{C}/{}^{12}\text{C}$ .

Carbon is present in the soil solid phase in the form of organic and inorganic carbon. Whereby the former is made up of the residues of living things in various states of decomposition as well as elemental carbon such as charcoal. Inorganic carbon on the other hand is mainly represented by carbonate containing minerals like calcite (Walthert et al. 2010). In addition to the total carbon (TC) content, TOC was determined by treating the samples with hydrogen chloride acid fumigation before combustion. The methodology used in this case was the stepwise-acidification method proposed by Walthert et al. 2010 and adjusted by S. L. Bellè and M. Schiedung (UZH).

For fumigation, each sample was weighed into 9x5 mm silver capsules, put in a titer plate and wet with 50 µl of 1 % HCl. Following, the open capsules were placed in a desiccator in vapour produced by 100 ml of 37 % HCl, for 8 hours. Since the samples did not contain high amounts of carbonates, no excessive foaming as described by Walthert et al. (2010) occurred (see Figure 9A and B). However, some minor foaming could be observed for the F3 samples between 30-60 cm. Subsequently, the open capsules were dried for 24 hours in a continuously vacuumised desiccator containing drying granules and subsequently in a vacuum oven at 32 °C and 200-300 hPa for 3 days. Immediately after removal from the oven, all capsules were transferred into 10x10 mm tin capsules and closed to avoid losing sample material, since the silver

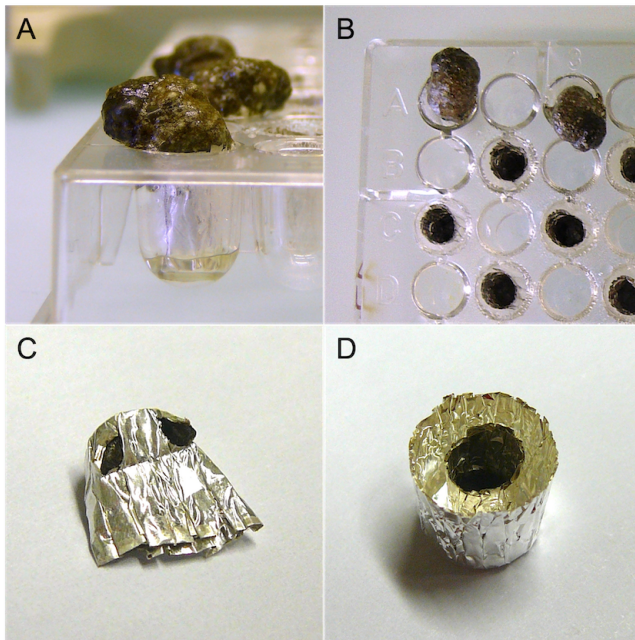


**Figure 9:** Methodical problems that might occur during fumigation: A) and B) Loss of sample due to excessive foaming of carbonates. C) Loss of sample due to ripping of brittle capsules after acid treatment. D) Repacking into larger capsules, to avoid sample loss and dirtying of Picarro. (Pictures used with permission from Walthert et al. 2010).

capsules became brittle from the acid treatment and could possibly break.

The amount of sample used for TC and TOC measurement depended on the carbon content of the respective sample. For TC measurements, bulk soil was weighed in at 12-15 mg, POM at 2-3 mg, S+A at 40 mg, and lastly, s+c at 5-6 mg. Further, TOC measurements were done with 25 mg for bulk soil, only 0.5-1 mg for POM, 80 mg for the S+A fraction and 12-15 mg for s+c. Moreover, the standards were weighed in at 12-15 mg for Chernozem and 2-3 mg for *Miscanthus* for both, TC and TOC measurements. In some cases only very little POM was available, so 0.5 mg were used and for samples with high carbon content, the bulk soil samples for TOC were reduced to 12-15 mg. Further, the 80 mg for S+A TOC measurements were weighed in as two separate 40 mg capsules and only combined in the larger 10x10 mm capsule for combustion. All measurements were run for a maximum of 900 seconds or until the CO<sub>2</sub> level dropped below 50 ppm.

#### 4.2.3 Diffuse reflectance mid-infrared Fourier transform spectroscopy

DRIFTS can provide a measure of SOC quality in different SOC pools (Calderón et al. 2011). This is done by measuring the absorbance of infrared light by a sample and extracting specific peaks of interest, which correspond to compounds such as lignin and cellulose. The ratio of the area under these peaks may then serve as a proxy for SOC quality and the partitioning of SOC into different pools (Laub et al. 2020). The absorption bands of interest were chosen based on previously identified bands (Chatterjee et al. 2012; Laub et al. 2020; Spaccini et al. 2001; Yeasmin et al. 2020) and consist of the peaks within the wavelength ranges 859-901 cm<sup>-1</sup> (aromatic compounds), 1210-1260 cm<sup>-1</sup> (cellulose), 1500-1510 cm<sup>-1</sup> (lignin), 1580-1660 cm<sup>-1</sup> (aromatic compounds) and 2800-3010 cm<sup>-1</sup> (aliphatic compounds). The derived ratios consisted of the cellulose:lignin as well as the aliphatic:aromatic1620 and the aliphatic:aromatic880 ratios. They were used as qualitative proxies for the ratio of fast-cycling to slow-cycling SOC or else SOC dynamics (Bellè et al. 2022; Laub et al. 2019).

Samples were measured using a Bruker Tensor 27 FT-IR spectrophotometer (Bruker, Switzerland) with the corresponding OPUS TM software. Thereby, the resulting spectra were a combination of 64 scans with a 4 cm<sup>-1</sup> resolution, ranging from 4000 to 400 cm<sup>-1</sup>. Before measuring the samples, potassium bromide was run as a background sample



**Figure 10:** Visualisation of the sample holder used for DRIFTS measurements.

to account for any atmospheric variations. Then, single channel measurements of the samples were run, baseline corrected and exported as dpt files. All samples were measured once and with a standard sample holder provided by the manufacturer. However, for some POM samples it was not possible to fill the standard sample holder, due to the available sample quantity. Hence, Thomas Keller (UZH) made a new sample holder, with smaller volume but equal surface area (see Figure 10).

The smaller sample holder used for the measurement of all POM samples had a volume of 17 mm<sup>3</sup> (r = 3.28 mm, h = 0.5 mm) and was made out of stainless steel. To ensure measurements would not be affected by the volume difference between the holders, I tested the new one using reference sample

material: *Miscanthus* and Chernozem samples were each measured ten times with the small and ten times with the standard sample holder. The order of measurements was determined randomly and the potassium bromide background was run with a standard sample holder. Results were tested using a one-sided paired t-test for each wavelength in Excel and discussed in the work group. In the case of *Miscanthus*, a significant influence could be detected between 770 and 860  $\text{cm}^{-1}$ , which corresponded to an aromatic C–H out-of-plane bend, O–H bending of phyllosilicates, Fe- and Al- oxides as well as Si–O bending of quartz (Yeasmin et al. 2017). This was close to the aromatic880 band of interest, but does not overlap with the integration limits of 850 to 910. Conversely, the chernozem results indicated a significant difference for the aliphatic carbon band with integration limits 2800-3010  $\text{cm}^{-1}$ . However, since *Miscanthus*, which is milled organic material, did not show any significant differences in the relevant areas, the small holder was used to measure the POM fraction samples (overview of significant differences in Figure 23).

### 4.3 Statistical analysis and data visualisation

Data produced with the Picarro CM-CRDS system (CRDS Picarro, Inc. 2020) was processed first in Excel, where data points were corrected for instrument drift between standards with a linear model. Further, carbon contents as well as isotopic ratio were calculated based on the measured results and drift correction. After computation, statistical analysis and data visualisation were carried out using R 2021.09.0 (R Core Team 2020). Firstly, differences in TOC concentration between sampling sites and depth per fraction were tested for normal distribution using the Shapiro-Wilk’s test as well as for homogeneity of variance (centre = mean) with the Levene’s test. In some cases data was transformed to meet the assumption of normal distribution using square root, logarithmic or 1/x transformation. Further, sampling sites were then compared using one-way analysis of variance (ANOVA) and a Tukey post-hoc test was applied for pairwise comparison. Additionally, the residuals of the linear models were again tested for normal distribution. However, the bulk soil samples as 45-60 cm were excluded from the linear model, since the data could not be transformed to fit a normal distribution using common transformation methods. And using a stronger transformation would put into question the statistical validity of the data. Additionally, few outliers significantly distorted the data distribution of the S+A fraction. Hence, one data point at 30-45 cm and two at 45-60 cm of sampling site F3 were removed from analysis. Therefore, the ANOVA could not be performed at those depths ( $n = 2$  and  $n = 1$  respectively). An overview of the results of statistical testing can be found in section A.2.1, in the appendix.

Secondly, the absorbance spectra produced using DRIFTS, were loaded into R as single dpt and merged into a workable data frame for further analysis. Using an adapted script by M. Schiedung, wavelength ranges of interest were extracted. Then, the ratios were calculated and their descriptive statistics exported as csv-file for plotting. Finally, Demyan et al. (2012) and Laub et al. (2020) proposed that the aliphatic and aromatic-carboxylate carbon bands of the DRIFTS absorbance spectra serve as proxy for fast and slow cycling carbon respectively. Hence, the correlations between TOC concentrations in fractions and DRIFTS band ratio were calculated using the Pearson correlation test



(linear, parametric). Some data was transformed to fit the assumptions of normal distribution see Figure 24). Further, the slow aromatic-carboxylate carbon was calculated based on Laub et al. (2020) through dividing the aromatic band area by the sum of the aromatic and aliphatic band areas:

$$arom1620cm^{-1}/(ali2930cm^{-1} + arom1620cm^{-1}) \quad (1)$$

and similarly, the fast cycling aliphatic carbon was calculated as follows:

$$ali2930cm^{-1}/(ali2930cm^{-1} + arom1620cm^{-1}) \quad (2)$$

The significance level for all above mentioned statistical analysis was 0.05 and plots were created using ggplot (Wickham 2016).



## 5 Results

### 5.1 Difference in carbon content between sampling sites

#### 5.1.1 Overview of total carbon and total organic carbon contents

The sample mass recovery from fractionation averaged at 91.7% and ranged from 84.4 to 97.6%. (see Table 4). Thereby, the values below 90% were mainly found with F4 (Vertisol on amphibolite), and between 45 and 60 cm for all sampling sites except F3. Similarly, the lowest carbon recoveries were found in the lower depth intervals. However, carbon recovery was generally above average for the Vertisols and the lowest values were mostly found with F1 (Lixisol) and F6 (Ferralsol), but also F2 (Lixisol) and F5 (shallow Ferralsol). Mean carbon recovery was 90.3%, but ranged from 64.1 to 115.1%. Hence, 17 samples with a carbon recovery under 80% or mass recovery below 85% were re-fractionated and remeasured with all methods. Results of mass recovery increased for 12 out of 17 samples and carbon recovery improved for 10 and decreased for 7 samples. Accordingly, 2 repeats were not included in the data set for analysis, since neither carbon nor mass recovery had improved.

**Table 2:** Overview of TC [%] (n = 3), TOC [%] (n = 6) and respective  $\delta^{13}\text{C}$  measurements for the bulk soil. An overview of the data for the fractions can be found in Table 5.

| Site | depth [cm] | TC [%]      | TC $\delta^{13}\text{C}$ [‰] | TOC [%]     | TOC $\delta^{13}\text{C}$ [‰] |
|------|------------|-------------|------------------------------|-------------|-------------------------------|
| F1   | 0-15       | 2.02 (0.04) | -27.04 (0.51)                | 2.18 (0.07) | -26.62 (0.34)                 |
|      | 15-30      | 0.77 (0.06) | -23.67 (0.29)                | 0.81 (0.04) | -23.07 (0.12)                 |
|      | 30-45      | 0.49 (0.06) | -23.31 (0.05)                | 0.54 (0.03) | -23.70 (0.16)                 |
|      | 45-60      | 0.46 (0.04) | -23.53 (0.35)                | 0.49 (0.02) | -22.79 (0.20)                 |
| F2   | 0-15       | 2.95 (0.10) | -27.34 (0.47)                | 3.15 (0.11) | -26.89 (0.31)                 |
|      | 15-30      | 1.68 (0.08) | -25.35 (0.23)                | 1.78 (0.09) | -24.91 (0.13)                 |
|      | 30-45      | 1.00 (0.11) | -23.63 (0.36)                | 0.99 (0.06) | -23.91 (0.20)                 |
|      | 45-60      | 0.67 (0.03) | -22.87 (0.28)                | 0.77 (0.01) | -22.32 (0.20)                 |
| F3   | 0-15       | 4.80 (0.38) | -28.99 (0.08)                | 4.49 (0.18) | -28.46 (0.10)                 |
|      | 15-30      | 2.01 (0.12) | -25.75 (0.41)                | 1.80 (0.09) | -25.94 (0.21)                 |
|      | 30-45      | 1.53 (0.30) | -21.35 (1.47)                | 1.05 (0.02) | -24.20 (0.23)                 |
|      | 45-60      | 2.10 (0.29) | -16.20 (1.05)                | 0.91 (0.05) | -22.72 (0.45)                 |
| F4   | 0-15       | 4.86 (0.03) | -26.14 (0.42)                | 4.16 (0.16) | -25.53 (0.22)                 |
|      | 15-30      | 2.83 (0.14) | -24.06 (0.56)                | 2.63 (0.10) | -24.91 (0.34)                 |
|      | 30-45      | 2.18 (0.10) | -22.70 (0.48)                | 1.94 (0.09) | -23.84 (0.31)                 |
|      | 45-60      | 1.77 (0.08) | -21.91 (0.34)                | 1.66 (0.01) | -22.35 (0.20)                 |
| F5   | 0-15       | 2.00 (0.19) | -28.09 (0.14)                | 1.74 (0.10) | -26.66 (0.23)                 |
|      | 15-30      | 0.95 (0.12) | -25.35 (0.28)                | 0.89 (0.10) | -25.01 (0.23)                 |
|      | 30-45      | 0.74 (0.11) | -25.07 (0.30)                | 0.70 (0.06) | -24.81 (0.19)                 |
|      | 45-60      | 0.59 (0.07) | -25.12 (0.39)                | 0.62 (0.04) | -25.00 (0.40)                 |
| F6   | 0-15       | 3.27 (0.12) | -26.90 (0.28)                | 3.15 (0.08) | -26.20 (0.29)                 |
|      | 15-30      | 1.84 (0.04) | -24.87 (0.12)                | 1.75 (0.05) | -25.07 (0.21)                 |
|      | 30-45      | 1.36 (0.09) | -24.72 (0.64)                | 1.25 (0.05) | -24.97 (0.38)                 |
|      | 45-60      | 1.26 (0.09) | -24.40 (0.39)                | 1.32 (0.05) | -24.50 (0.25)                 |

Differences between TC and TOC contents were generally small and within the standard error (SE) of the measurements. Notably, some results indicated higher values of TOC than TC, especially the S+A

fraction (see Table 5). For example the bulk soil data for F5 at 30-45 cm had a TC value of  $0.74 \pm 0.11\%$  and TOC resulted in  $0.70 \pm 0.06\%$ . Also, F2 at 15-30 cm had a TC content of  $1.68 \pm 0.08\%$  and a TOC content of  $1.78 \pm 0.09\%$  (see Table 2). This might be attributed to field heterogeneity, sample variability and a low number of replicates instead of the loss of inorganic carbon. Conversely, F3 showed a significant decrease in carbon after fumigation from  $1.53 \pm 0.30\%$  and  $1.77 \pm 0.08\%$  to  $1.05 \pm 0.02\%$  and  $0.91 \pm 0.05\%$  for the third and fourth depth interval respectively. Additionally, the isotopic ratio indicated a clear decrease from  $-16.20 \pm 1.05\text{‰}$  to  $-22.72 \pm 0.45\text{‰}$  at 45-60 cm. This loss might be attributed to inorganic carbon, since F3 contained carbonates in the form of secondary minerals (calcite).

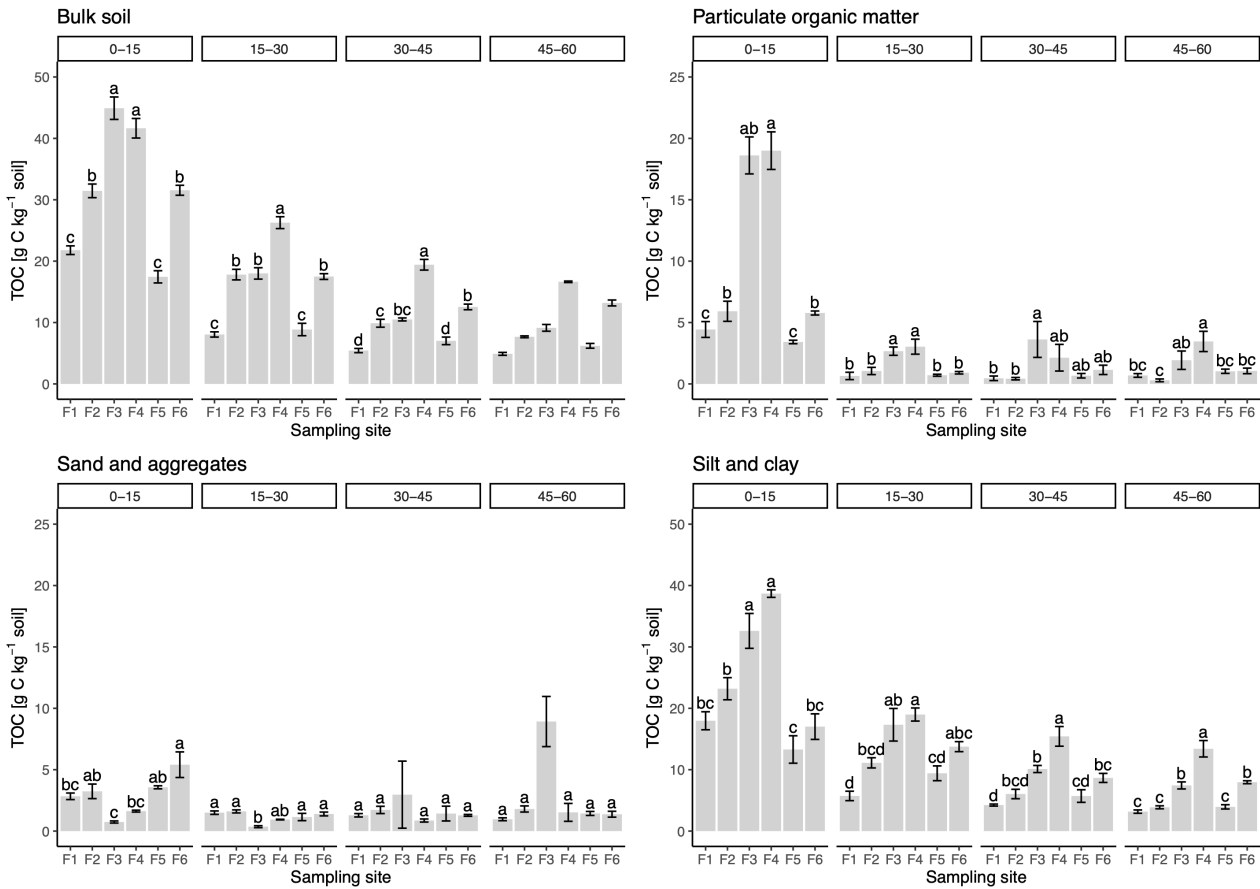


**Figure 11:** Distribution of TOC concentration [g C kg<sup>-1</sup> soil] between sampling sites per depth. Values represent the mean ( $n = 6$  for bulk soil and  $n = 3$  for fractions) and error bars the standard error (SE). Letters above the bars indicate the significance levels of Tukey posthoc pairwise testing at  $p < 0.05$ . Some data was transformed to ensure normal distribution. Further, the bulk soil at 45-60 cm and some outliers of F3 (S+A fraction) were excluded from the linear model (see section 4.3). Note the different y-axis scales. Results of residual statistical testing can be found in Table 7.

### 5.1.2 Difference in total organic carbon between sampling sites with depth

Figure 11 showed that the TOC concentration is generally highest in the upper 15 cm of the soil in all fractions and gradually decrease with depth for the bulk soil as well as the s+c fraction. The s+c

fraction closely resembled the results obtained for the bulk measurements. Conversely, for POM and S+A the decrease was more abrupt and most notable between the first and second depth interval, while TOC remained similarly low between 15-60 cm. Further, differences between sampling sites were larger between 0-15 cm, as can be seen from the indicated significance levels in Figure 11. In the case of the s+c fraction for example, the Vertisols were significantly different from the other soil types between 0-15 cm, but not at lower depths. Moreover, differences in TOC between sampling sites were lowest for the POM fraction and especially the S+A fraction. Here, little difference was visible between sampling site or soil types. Although, the Vertisols (F3 and F4) did generally have higher TOC than the Lixisol and Ferralsols and F1, F2 (Lixisols) and F5 (Ferralsol) shared similar TOC concentrations over all fractions and depths. However, the SE of sampling sites F3 and F4 was comparatively large below 30 cm for both the S+A and POM fractions. Further, F3 and F4 had lower TOC values for S+A at 0-15 cm as compared to the other samplings sites, but distinctly higher values for POM at the same depth.

As can be gathered from Figure 12, the majority of TOC was present within the s+c fraction. Values ranged from 77.2-97.0% of TOC, followed by POM at 1-17.7% and S+A at 0.8-13.3%. This held true for all sampling sites and depth intervals, although its proportion was largest at 15-30 cm and then decreased with depth. Further, POM was largest at 0-15 cm, which was confirmed in Figure 11. Conversely, S+A seemed to be relatively constant throughout all depths for the Lixisols and Ferralsols, but slightly increased in proportion at 45-60 cm. Conversely, the S+A fraction only made up a very small part of the Vertisols between 0-30 cm, then slightly increased for F4 and increased notably for F3, with a visible jump between the third and fourth depth interval.

## 5.2 Total organic carbon and $\delta^{13}\text{C}$ trends with depth

### 5.2.1 Bulk soil

Figure 13a showed an overall decrease in TOC content with depth, whereby the difference was largest between the first and second depth interval and decreased less abruptly deeper in the profile. The curve shape was comparable between all soil types and TOC ranged from approximately 4.5 to 0.5%, whereby the Vertisols showed higher values in the top 15 cm as compared to the other soils. Further, the TOC values were slightly lower for F1, F3 and F5 as compared to F2, F4 and F6 respectively.

Measured  $\delta^{13}\text{C}$  values indicated an overall increase with depth, that is, less negative values. F1 and F2 had very comparable curves, except for the second depth interval, where F1 was about 2‰ higher. Similarly, F3 and F4 had similar curve shapes starting at 30 cm, whereas the first depth interval showed a difference of approximately 3‰. Lastly, the  $\delta^{13}\text{C}$  values of F5 and F6 were almost identical. Compared to the other soils however, the values did not change much from the second to fourth depth and the entire profile therefore lied within -27 to -24‰.

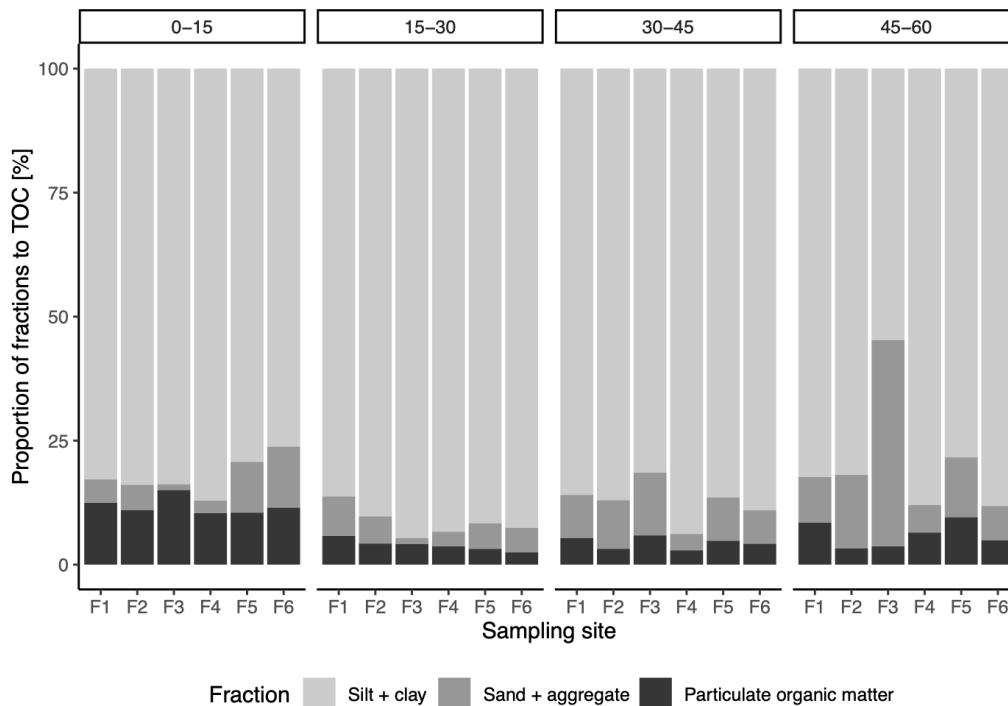


**Figure 12:** Proportion of each soil fraction to the TOC of the bulk soil, normalised to 100 %.

### 5.2.2 Particulate organic matter

The TOC in the POM fraction was characterised by very high carbon contents as compared to the other fractions as well as large variability (see Figure 13b). While the values for F3 and F4 as well as F5 and F6 were comparable, F1 showed a stronger decrease with depth and a jump from the second to third interval as compared to F2. Notably, F4 recorded an increase in TOC between the first and second depth and F5 from the second to the third depth interval.

The  $\delta^{13}\text{C}$  signals for all sampling sites except F4 were characterised by an initial increase until the second (F3, F5 and F6) or third (F1 and F2) and subsequent decrease until the fourth depth interval. Such a decrease could not be observed in the bulk sample or any other fraction. Conversely, the  $\delta^{13}\text{C}$  trend for sampling site F4 first decreased and then increased starting at 15-30 cm. Further, the difference between the Vertisols was large compared to the other soil types.

### 5.2.3 Sand and aggregates

Notably, the TOC content was very small in the S+A fraction. Additionally, there was little change with depth for all sampling sites except F3 and the differences between first and second depth of F5 and F6. The first showed a very strong increase after the second depth interval: Values increased from close to 0 to over 2% TOC. Additionally, the SE increased too, which was in line with the presence of calcite for the third and fourth depth of site F3. The latter had visibly higher TOC concentrations between 0-15 cm as compared to the other four soils.

Overall, the  $\delta^{13}\text{C}$  signal increases with depth and was lower than for the other fractions or the bulk samples. While the sampling sites F1 and F2 as well as F5 and F6 generally behaved very similar, sites F3 and F4 showed more variable results. Especially, F3 measured a very high signal of approximately  $-10\text{‰}$  at 45-60 cm and covered a broader range of values than F4, even in the first three depth intervals, while F4 remained relatively constant between 0-45 cm. Further, the SE for F3 was large compared to other  $\delta^{13}\text{C}$  signals. Conversely, values remained very constant between the second and fourth depth for sites F1 and F6.

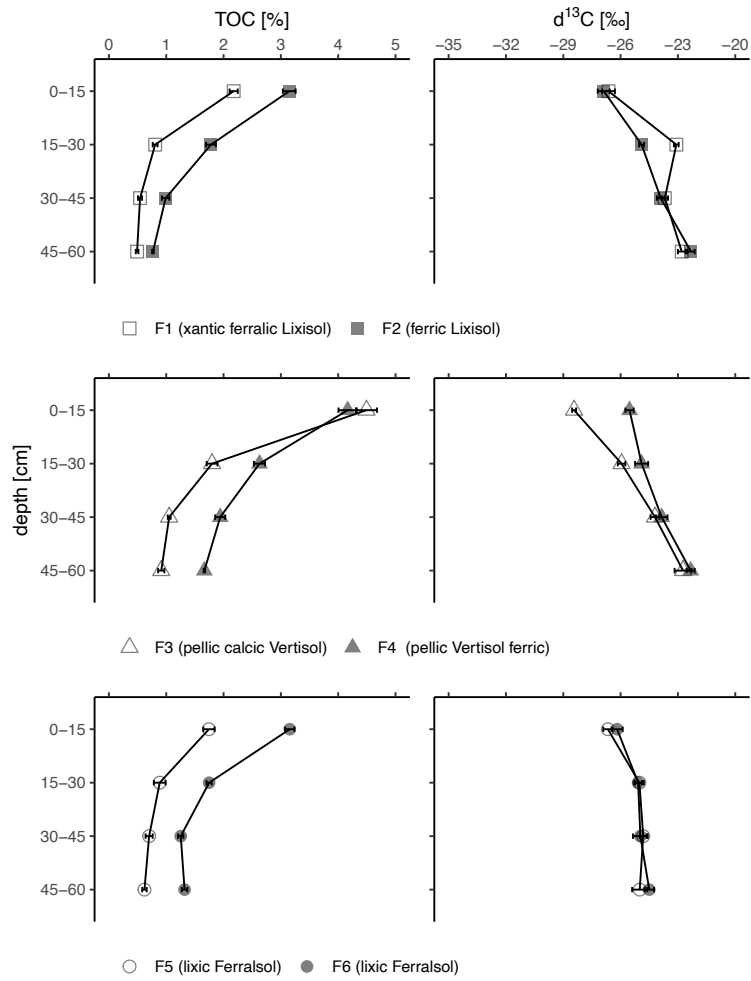
#### **5.2.4 Silt and clay**

Overall we observed high TOC contents and similar curve shapes over all sampling sites: All decreased with depth, whereby the strongest difference could be seen from the first to the second depth interval. Further, the curves compared well with the bulk measurements, given that the s+c fractions made up the majority of the TOC (see Figure 12). This could be seen in the prevalent jumps between first and second depth of sites F1 to F4, which were less pronounced in sites F5 and F6. Moreover, sites F2, F5 and F6 had higher TOC contents than their paired samples. However, values lied closer together and were slightly higher than for bulk. As for the TOC values, the  $\delta^{13}\text{C}$  signal was close to the bulk samples'. It decreased with depth and values were very close for the individual soil pairs. Only sampling sites F3 and F4 showed some difference in the 0-15 cm interval.

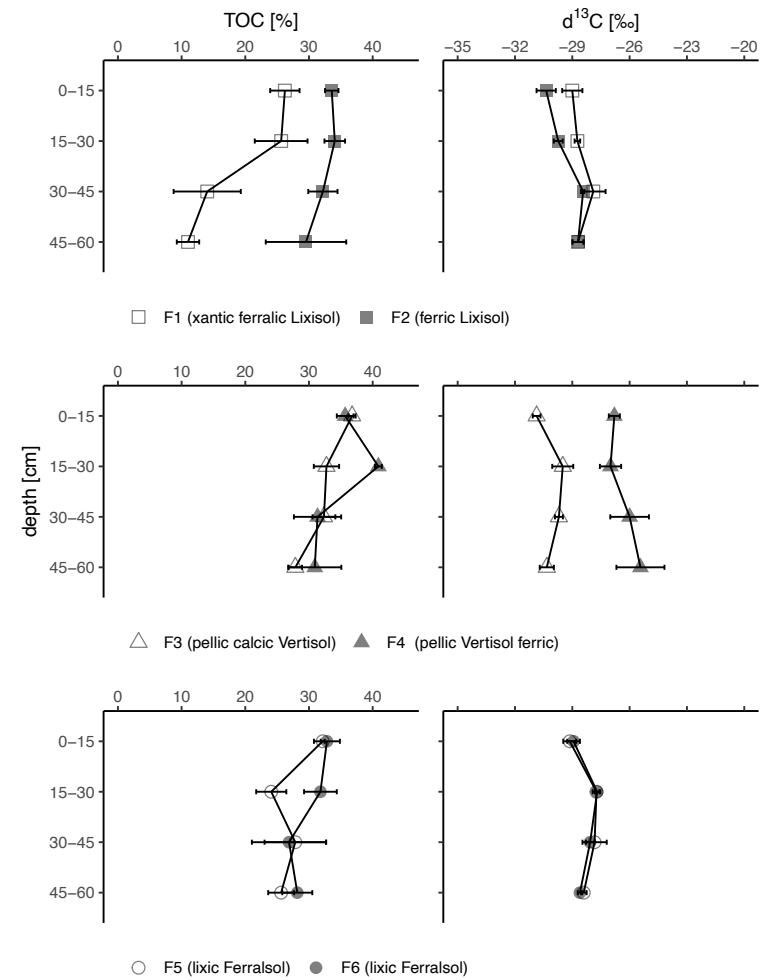
### **5.3 Diffuse reflectance mid-infrared Fourier transform spectroscopy**

#### **5.3.1 Bulk soil**

Curve shapes were similar for each ratio for the Lixisols and Ferralsols, but differed for the Vertisols, especially for the cellulose:lignin ratio. The ratio remained relatively constant with depth, with only a slight increase after 30 cm for F1, F2, F5 and F6. Conversely, the contribution of cellulose increased between the first and second depth interval for both Vertisols, F3 and F4. It continued to increase visibly after 30 cm for F4 but decreased for F3. Moreover, F6 showed a slight decrease between the third and fourth depth. Further, the aliphatic:aromatic<sub>1620</sub> curves were within the same range for most sampling sites, and showed a slight decrease in aromaticity with depth, that is an increase in ratio. However, the Vertisols did not change much with depth and for F3 the ratio slightly decreased after 30 cm. Additionally, F6 did show a slight increase with depth but no change after 45 cm. Lastly, the curves for the aliphatic:aromatic ratio at  $880\text{ cm}^{-1}$  showed a slight decrease in ratio from the first to second depth interval, and then a slight increase with depth for F1, F2 and F5. However, F6 did not change much with depth but showed a comparable decrease between the first and second depth to F5. Although F6 had a visibly higher ratio than F5. Conversely, both Vertisols gradually decreased with depth and had overall higher values than the other soil types.

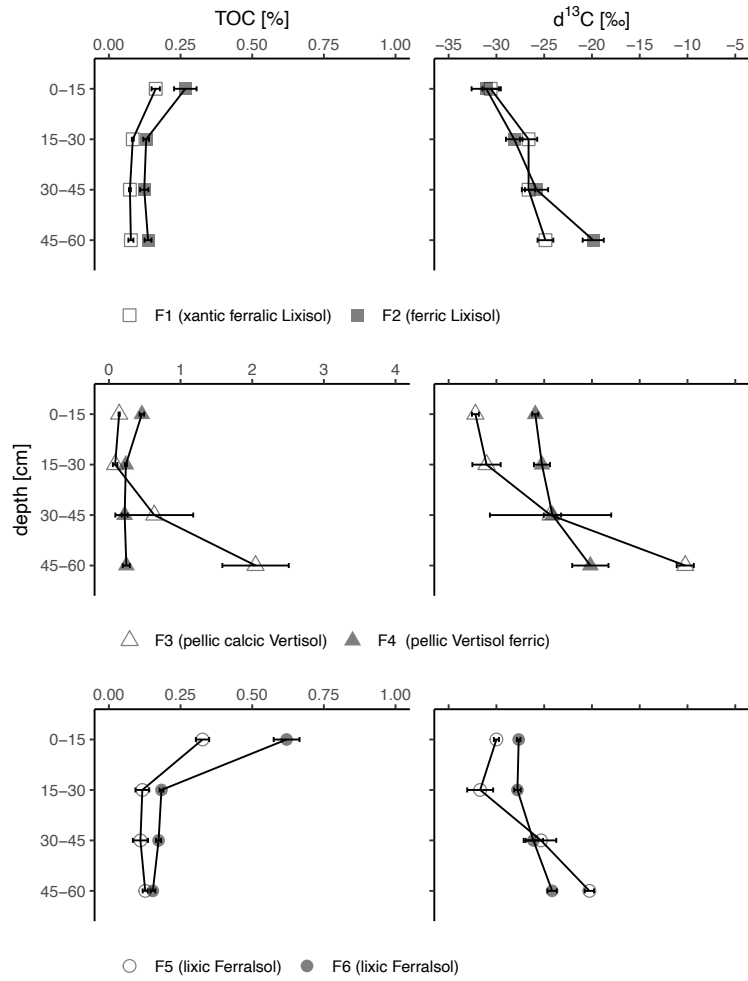


(a) TOC [%] distribution and carbon isotopic ratio  $^{13}C/^{12}C$  [‰] of the bulk soil (< 2 mm) with depth.

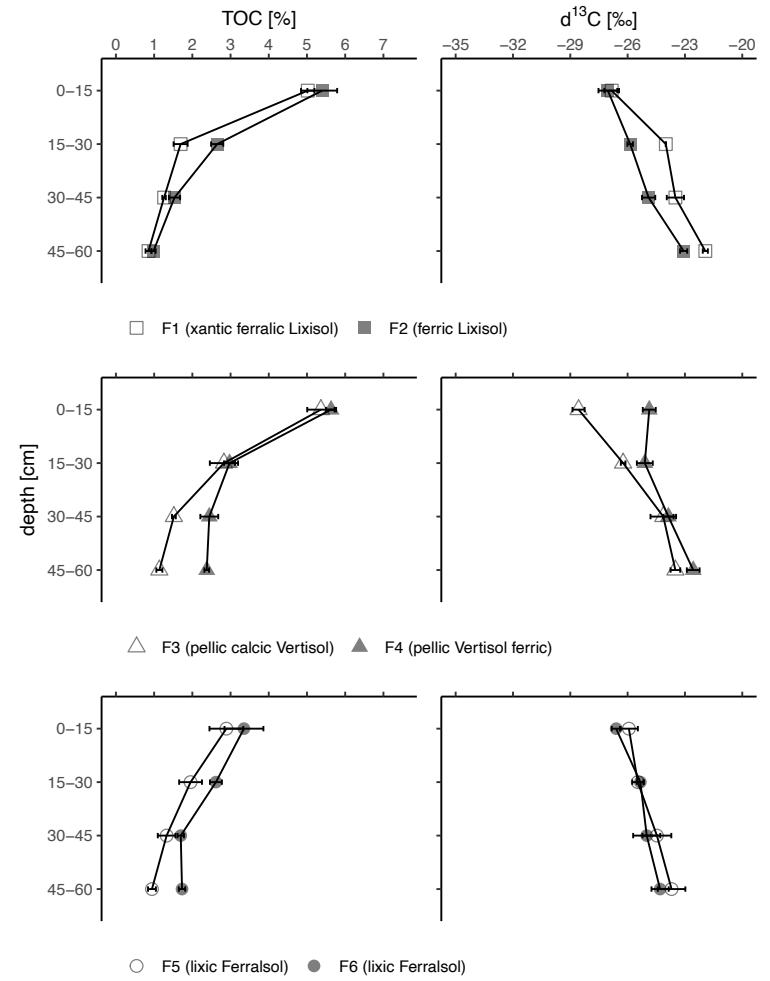


(b) TOC [%] content and  $^{13}C/^{12}C$  [‰] of the POM fraction with depth.

**Figure 13:** Total organic carbon content (TOC) content [%] and carbon isotopic ratio  $^{13}C/^{12}C$  [‰] by depth for each sampling site.



(c) TOC [%] distribution and  $^{13}C/^{12}C$  [‰] of the S+A fraction with depth.



(d) TOC [%] distribution and  $^{13}C/^{12}C$  [‰] of the s+c fraction with depth.

**Figure 13:** Total organic carbon content (TOC) content [%] and carbon isotopic ratio  $^{13}C/^{12}C$  [‰] by depth for each sampling site.

### 5.3.2 Particulate organic matter

Generally, the cellulose:lignin ratios were low for POM and close to the ones of S+A with exception of F4 at 0-15 cm, which was notably higher but also had a large SE compared to other measurements. The aliphatic:aromatic<sub>1620</sub> ratio did not change much with depth and the curves were very close to each other over all sampling sites. Conversely, the aliphatic:aromatic<sub>880</sub> ratio showed the largest variability between soil types and over all sampling sites. The Lixisols had values around 15, while the Ferralsols were more aromatic with most values lying below 10. Next, the Vertisols differed notably, as F4 had values around 10, while F3 decreased from 52 to 15 with depth. Further, F1 and F2 showed an initial increase in ratio from the first to the second depth. F1 continued to decrease further, while F2 remained relatively constant between 30-60 cm. Moreover, F4 and F6 showed similar patterns of decrease, then increase with depth, although values were higher for F4. Notably, aromaticity remained stable with depth for F5. Overall, the aromaticity of the POM fraction was approximately a factor 10 lower than for the other fractions or the bulk samples.

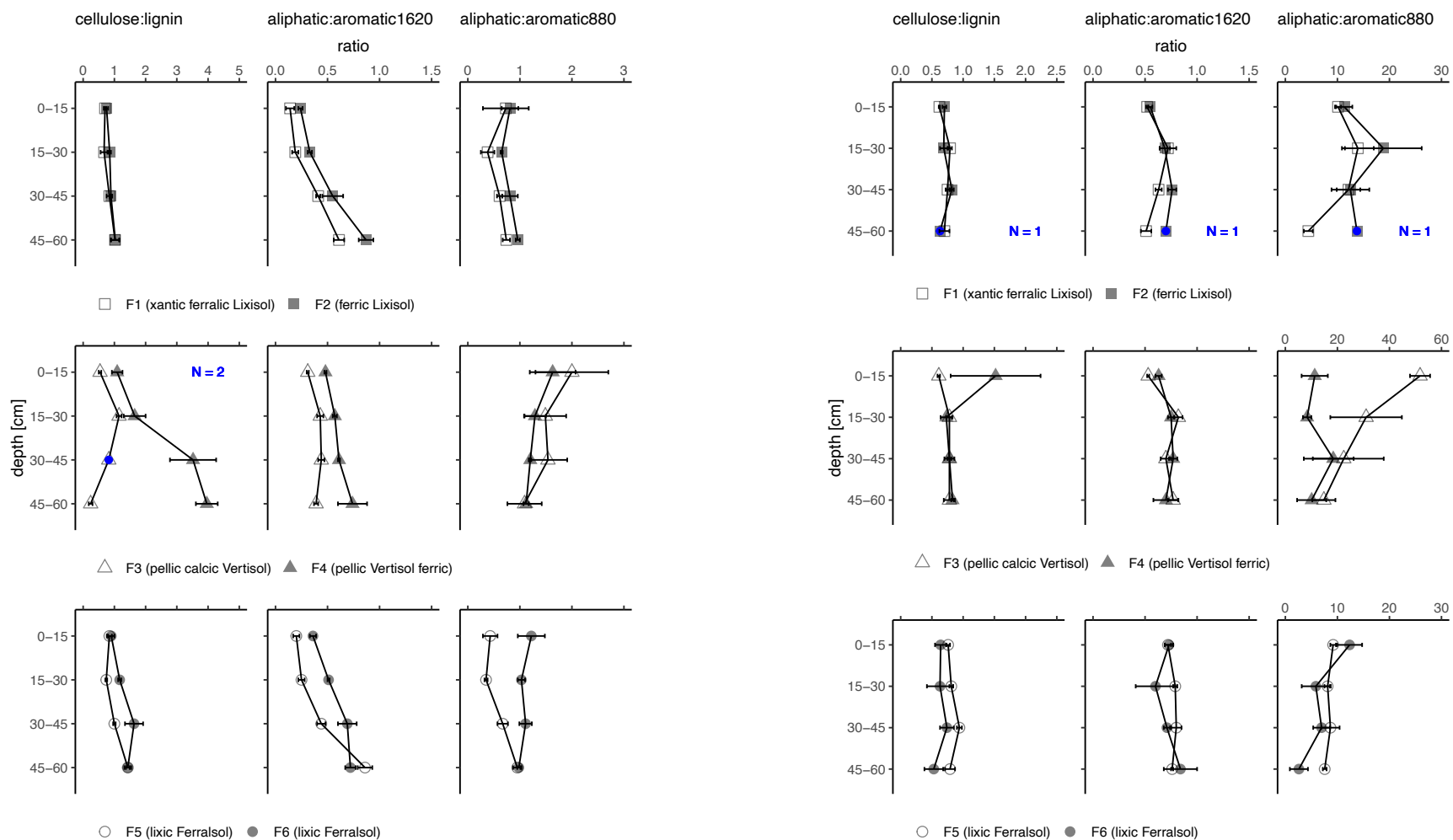
### 5.3.3 Sand and aggregates

In the case of the S+A fraction, trends for all ratios were similar with depth over all sampling sites: Little change with depth in case of the cellulose:lignin ratio and a slight increase with depth for the aliphatic:aromatic ratios. F1 and F2 behaved very similar over all ratios and only showed some difference at 45-60 cm: F2 slightly increased in lignin and did not change for aliphatic:aromatic<sub>880</sub>. However, F1 did not change with depth for the cellulose:lignin ratio, but increased in the aliphatic:aromatic<sub>880</sub> ratio. The Vertisols too behaved similarly, with no strong changes in cellulose:lignin ratios but a stronger increase in aliphatic:aromatic between the third and fourth depth and large SE at 45-60 cm. Lastly, F5 and F6 were very similar over all three ratios, with exception of F6 at 45-60 cm, where the cellulose:lignin ratio suddenly increases from close to 0 to 3.5. Overall, the S+A fraction showed the least variation between sampling sites and soil types.



#### 5.3.4 Silt and clay

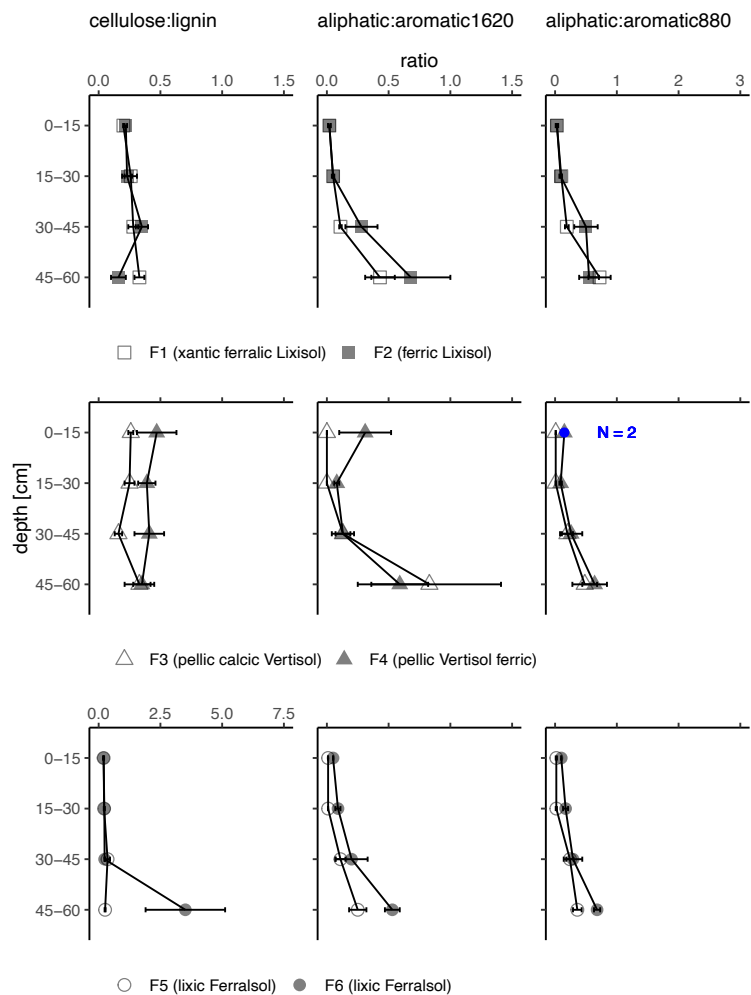
Within the s+c fraction, there were generally little opposing trends between sampling sites of the same soil type: The curve shapes and values were almost identical for the aliphatic:aromatic<sub>1620</sub> ratios over all depths. That is, values were very constant and at about the same range as POM, but higher than the S+A fraction and bulk samples. Similarly, the aliphatic:aromatic<sub>880</sub> ratios were higher for the s+c fraction than S+A and bulk, but not as high as POM. Except for site F6 at 45-60 cm, which was a notable outlier and in the range of POM values. Further, F3 and F4 had larger SE for the measurements of aliphatic:aromatic<sub>880</sub> ratio and a more visible decrease with depth than the Lixisols or the Ferralsols, which did not change with depth. In the case of the cellulose:lignin ratios there was more variability in curve shape than for bulk or S+A as well as a much higher increase of cellulose with depth and higher values overall. Notably, the cellulose:lignin ratio decreased between the third and fourth depth for F1, F4 and both Ferralsols, while it continued to increase for F1 and F3. Additionally, there was little change between 0-30 cm.



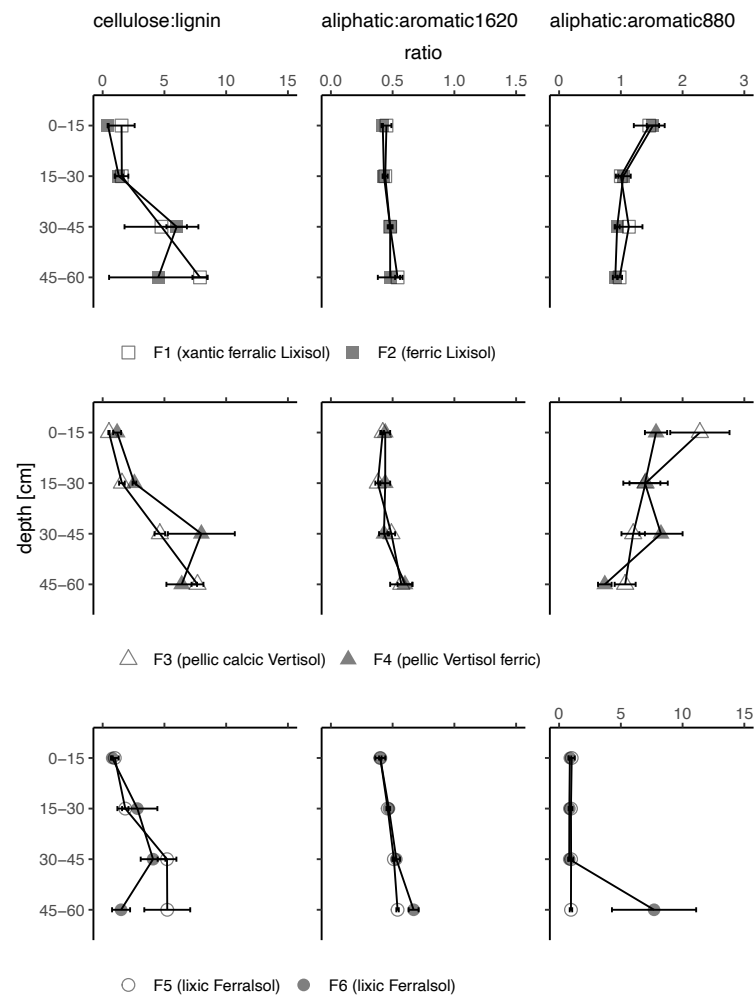
**(a)** Compound ratios of cellulose to lignin and aliphatic to aromatic carbon within the bulk soil. In blue: One outlier was removed in the cellulose:lignin ratio for F3 at 30-45 cm ( $n = 2$ ).

**(b)** Compound ratios of cellulose to lignin and aliphatic to aromatic carbon within the POM fraction. In blue: POM could not be measured for two out of three samples at in F2 at 45-60 cm ( $n = 1$ ).

**Figure 14:** Compound ratios derived from DRIFT spectral analysis, by depth for each sampling site. The selected absorbance bands were:  $859-901\text{ cm}^{-1}$  (aromatic compounds),  $1210-1260\text{ cm}^{-1}$  (cellulose),  $1500-1510\text{ cm}^{-1}$  (lignin),  $1580-1660\text{ cm}^{-1}$  (aromatic compounds) and  $2800-3010\text{ cm}^{-1}$  (aliphatic compounds).



(c) Compound ratios of cellulose to lignin and aliphatic to aromatic carbon within the S+A fraction. In blue: One outlier was removed in the aliphatic:aromatic880 ratio for F4 at 0-15 cm ( $n = 2$ ).



(d) Compound ratios of cellulose to lignin and aliphatic to aromatic carbon within the s+c fraction.

**Figure 14:** Compound ratios derived from DRIFT spectral analysis, by depth for each sampling site. The selected absorbance bands were:  $859-901\text{ cm}^{-1}$  (aromatic compounds),  $1210-1260\text{ cm}^{-1}$  (cellulose),  $1500-1510\text{ cm}^{-1}$  (lignin),  $1580-1660\text{ cm}^{-1}$  (aromatic compounds) and  $2800-3010\text{ cm}^{-1}$  (aliphatic compounds).

## 5.4 Ratio of labile to stable compounds

The ratio of aliphatic to aromatic carbon at  $1620\text{ cm}^{-1}$  did not have a significant relationship to the ratio of hypothesised fast to slow carbon fractions proposed by Laub et al. (2020) and neither did the reverse suggested by Demyan et al. (2012) (see Table 3). However, the individual variables did correlate: The slow carbon fraction, that is the S+A plus s+c fractions, showed a low positive correlation with the aromatic carbon band at  $1620\text{ cm}^{-1}$  significant. Further, the fast cycling fraction POM showed a negative relation with the aliphatic carbon band. However, the correlation was weak ( $R = -0.288$ ).

**Table 3:** Overview of correlation tests between slow and fast cycling DRIFT compounds and carbon fractions.

| variables                   | p-value | corr.coef |
|-----------------------------|---------|-----------|
| ali:arom1620, labile:stable | 0.171   | -0.163    |
| arom1620:ali, stable:labile | 0.171   | 0.163     |
| fast, POM                   | 0.014   | -0.288    |
| slow, S+A + s+c             | 0.001   | 0.375     |

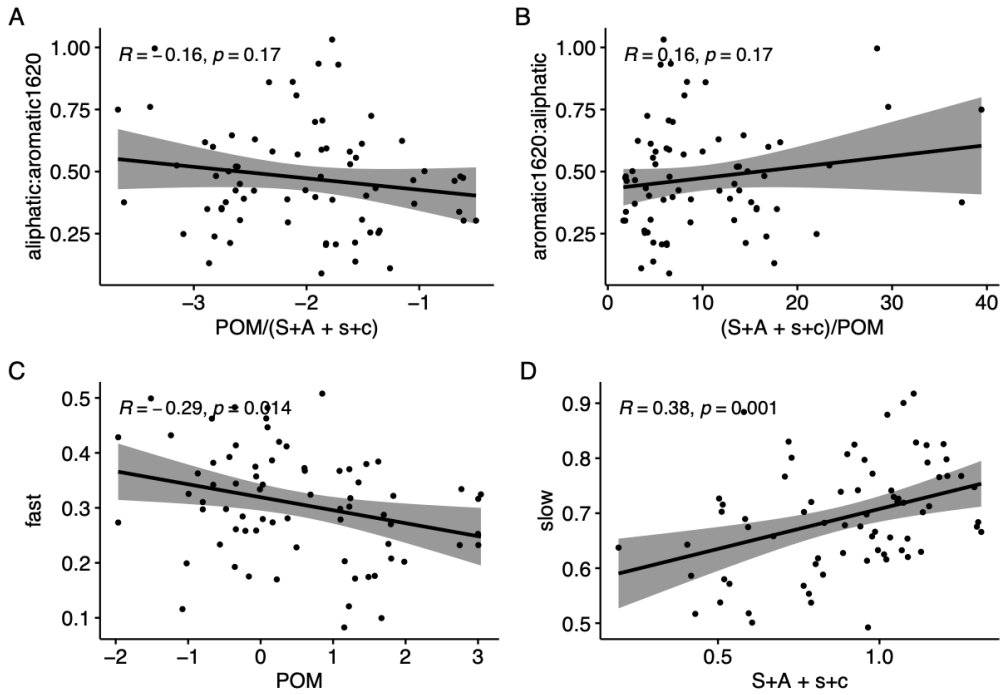


**Figure 15:** Correlation between the DRIFT band ratios of aliphatic and aromatic carbon with labile and stable SOC pool respectively. A corresponds to the DRIFTS stability index defined by Laub et al. (2020). B is based on the correlation of stable to labile SOC proposed by Demyan et al. (2012). C shows the Kendall correlation between the fast cycling carbon (see equation 2 in section 4.3) and the labile fraction (POM). D shows the Pearson correlation between the slow cycling carbon (see equation 1 in section 4.3) and the stable carbon fractions (S+A and s+c).

## 6 Discussion

The composition of SOC under tropical forests is understudied. Yet, their importance for the global carbon cycle is significant. Therefore, it is crucial to understand how soils under tropical forest will react to changes in climate or land use (Nottingham et al. 2020). By combining fractionation with measures of TOC,  $\delta^{13}\text{C}$  and DRIFTS, the vertical distribution of SOC in three important soil types (Kögel-Knabner and Amelung 2021), as well as its stability (Wang et al. 2017) could be examined. Further, the assessment of individual carbon fractions allowed to evaluate the principal mechanism of SOC stabilisation and the relative importance of more stable or labile carbon pool in the respective soils. Moreover, the ratios of chemical compounds, together with measures of  $\delta^{13}\text{C}$ , gave indication not only towards the degree of decomposition, but also the source of SOC.

### 6.1 General patterns

Measures of TOC concentration [ $\text{g C kg}^{-1}$  soil] decreased strongly after the first depth interval and remained similarly low after 30 cm. This fits the values found by Lorenz et al. (2009) for Inceptisols and Entisols under secondary, deciduous forest in Costa Rica. They found the highest TOC concentrations in the first 10 cm of the soil (51 [ $\text{g C kg}^{-1}$  soil]) and decreasing values between 26 and 12 [ $\text{g C kg}^{-1}$  soil] until 50 cm depth (Lorenz et al. 2009). Since above ground litter input is gradually incorporated into the surface of the soil, the first centimetres contain the largest amount of humus (Subashree et al. 2019). Although, the Vertisols contained more TOC throughout, which is in line with findings from Pal (2019), who show Vertisols amongst the soil types with highest SOC values.

Additionally, the TOC content [%] decreased with depth for all soils, which was most strongly reflected in the values of the s+c fraction and can be attributed to an increasing proportion of older, more processed SOC (Wang et al. 2017). Although, the TOC content of the POM fraction decreased with depth as well, the values remained significantly higher than the s+c fraction, since it contained less decomposed organic matter (Curtin et al. 2019). Conversely, the S+A fraction only contained little TOC, and primarily in the first 15 cm, whereas it remained relatively stable between the second and fourth depth interval. This has also been found for the S+A fraction in temperate forests (Christensen 2001) and can be attributed to the weak binding capacity of primary particles and low amount of aggregates (mostly dispersed during fractionation). However, its aromaticity decreased slightly with depth, which could be attributed to decreasing aggregation with depth and hence decreased presence of stabilised carbon (Subashree et al. 2019). Instead, aggregation might be influenced by new SOC input. Moreover, the TOC values found for POM and s+c fit well with the light fraction (LF) and heavy fraction (HF) identified by Wang et al. (2017) for secondary and natural tropical.

The isotopic signal of the first two depth intervals was consistent with those of natural and secondary forest found by Wang et al. (2017) for the first 20 cm. After which the values decreased substantially for F1-F4, but remained constant for the Ferralsols, indicating an increasing degree of decomposition with depth. Alternatively, less negative  $\delta^{13}\text{C}$  values might also indicate past inputs of  $\text{C}_4$ -vegetation such as grass (Bellè et al. 2022; Staddon 2004). Including data on compound chemistry, allowed to further

detangle and interpret the  $\delta^{13}\text{C}$ . The aromatic:aliphatic880 ratio showed higher values of aromaticity at depth for samples F3, F4 and F6, indicating increasing microbial decomposition, whereas the signal was slightly increasing at the other sampling sites. This might indicate the input of fresh organic matter from deep rooting shrub vegetation, such as *L. camara* (Subashree et al. 2019).

In all soils and depths, the s+c fraction contained the highest proportion of TOC, followed by POM and S+A. Although the relative importance of POM decreased with depth. This is in line with many studies (e.g. Buettner et al. 2014; Helfrich et al. 2007; Jindaluang et al. 2013; Poeplau et al. 2013; Telles Rodrigues et al. 2022) who found most TOC in the mineral-associated or s+c fraction and only a small pool of POM (Christensen 2001; Curtin et al. 2019). Further, the SOC fractions were increasingly enriched in  $\delta^{13}\text{C}$  in the following order:  $\text{POM} < \text{S+A} < \text{s+c}$ . Accordingly, the aliphatic:aromatic880 ratio confirmed an increasing aromaticity of those fractions and hence increasingly processed SOC. This corresponds to the order of fraction formation proposed by Gunina and Kuzyakov (2014), who found that density fractions were enriched as follows: free POM < light occluded POM < heavy occluded POM < mineral fraction. Further, it connects the SOC fractions to their hypothesised stability. Turnover times of carbon are longer in the s+c fraction than in the coarse (S+A) or light (POM) fractions (Blume et al. 2016).

## 6.2 Differences in soil organic carbon between sampling sites

Given the general characteristics of the three soil types, the lowest concentrations of carbon were expected in the Lixisols (F1, F2), followed by the Ferralsols (F5, F6) and the Vertisols (F3, F4). This was based on the assumption, that the latter would stabilise most carbon via mineral association with clay, mainly smectite and via peloturbation. Further, the Lixisols and Ferralsols would both stabilise some SOC with clay, however, mainly kaolinite. Additionally, Ferralsols should bind significant amounts of SOC through ligand exchange with oxides (Blume et al. 2016), since pH was shown to be acidic (5.1-5.5) by Bellè et al. (2022).

### 6.2.1 Vertisols

The TOC concentration [ $\text{g C kg}^{-1}$  soil] of the Vertisols was significantly higher in all fractions at 0-15 cm, except S+A. Thereby, F4 generally remained higher than F3 throughout the entire profile, which suggests that smectite had a higher capacity to store SOC. While F4 (Vertisol on amphibolite) consisted mostly of smectite, F3 (Vertisol on gneiss) also contained significant amounts of kaolinite and interstratified kaolinite-smectite (Bellè et al. 2022) which have lower specific surface areas and charge (Blume et al. 2016). However, the s+c fraction contained similar amount of TOC, at least in the first two depth intervals. Additionally, multiple studies found no significant difference between the carbon stabilisation capacities of Vertisols with varying clay assemblages (Kögel-Knabner and Amelung 2021, and studies mentioned therein) or general correlation between clay mineralogy and SOC variability in the tropics (Pulido-Moncada et al. 2018). Yet, Bellè et al. (2022) found higher concentrations of iron ( $\text{Fe}_2\text{O}_3$ ) at F4 than F3 (see Table 2 in Bellè et al. 2022), which could explain the larger amount of TOC, especially at lower depths. Conversely, Rumpel and Kögel-Knabner (2011) indicate, that the

sorptive capacity of oxides might be reduced under near neutral soil environments. Additionally, the presence of carbonates at F3 could also lead to higher contents of organic carbon, due to their capacity to stabilise SOC (Rowley et al. 2018), which was most visible in the TOC concentration of the S+A fraction.

Peloturbation could be confirmed at both Vertisol sites. On one hand, the POM aliphatic:aromatic880 ratio of F3 decreased significantly with depth, suggesting an increasing degree of decomposition, while F4 remained relatively stable. However, POM at F3 was much more aliphatic than any other sampling site, indicating largely unprocessed SOC at depth. On the other hand, the bulk  $\delta^{13}\text{C}$  did not indicate large differences in the degree of decomposition with depth at F3, although the source of above ground litter input might have varied: F4 bulks soil showed a less negative isotopic signal at 0-15 cm, and an overall  $\delta^{13}\text{C}$  enriched POM fraction, which could be attributed to a higher proportion of  $\text{C}_4$ -grass input (Staddon 2004). Furthermore, the bulk soil aliphatic:aromatic1620 ratio suggested more aliphatic vegetation at F4, as well as larger amounts of cellulose. Both are indicative of a more grass-dominated vegetation, relative to F3.

The cellulose:lignin ratio of the bulk soil showed a strong difference between the two Vertisol sites after 30 cm. While the values decreased after 30 cm for F3, they visibly increased for F4, indicating more grass-derived litter input in the past or the preferential stabilisation of cellulose over lignin. Such high cellulose values were otherwise only measured for the s+c fraction, although the differences between the two Vertisols were small. The low cellulose:lignin ratio at F3 is confirmed by the bulk DRIFT spectra at 30-45 cm (see Figure 16): The peak at  $1245\text{ cm}^{-1}$  lies close to 0, which suggests mainly the input of woody SOC. Alternatively, termites might influence the SOC composition at the site (Jouquet et al. 2016).

The proportion of SOC in the S+A fraction increased significantly, at the expense of s+c, for the third and fourth depth interval at F3. This might be attributed to incomplete fumigation of carbonates or the occurrence of sandy loam in the valley bottom, as described by Barbiéro et al. (2010). However, high values of TOC concentration with large SE, indicated that fumigation did not work in full, which was confirmed by a high  $\delta^{13}\text{C}$  signal (see Table 2). Since no sample had foamed excessively during treatment with HCl, only one round of acid fumigation was applied, as opposed to the two rounds suggested by Walthert et al. (2010). Subsequently, not all SIC was removed because of the calcite's large specific surface area (Blume et al. 2016). This effect was especially prominent in the S+A fraction and to a lesser extent in the s+c section, suggesting that carbonates play an important role in aggregation (Rowley et al. 2018) and to a lesser extent in the adsorption of organic acids onto smectite (Blume et al. 2016).

### 6.2.2 Lixisols and Ferralsols

TOC concentrations of the sampling sites F1 and F5 as well as F2 and F6 were more similar to each other than sites of the same soil type. Sampling sites F1 and F5 had significantly lower TOC values than the other four sites for all depth intervals (see Figure 11). This corresponded to the soil texture

reported by Bellè et al. (2022): The lowest values for clay and highest values for sand were found at those sites. However, both Ferralsols showed a relatively strong decrease in TOC content of the S+A fraction between the first and second depth interval, as well as an initial decrease in  $\delta^{13}\text{C}$ , which was not visible in the Lixisols and might be attributed to the aggregation of partly degraded plant residues found in the forest floor O horizons at the sites (Bellè et al. 2022, data not shown).

The bulk soil  $\delta^{13}\text{C}$  signal of the Ferralsols suggested the input of fresh carbon at depth through root and exudates. Yet, this is questionable, since that would mean higher concentrations of lignin and aliphatic material as compared to the topsoil (Rumpel and Kögel-Knabner 2011), which was not the case. Although lignin is enriched compared to the other sampling sites. However, Bellè et al. (2022) also reported termites at F6 (and F3), which could further influence the distribution of non-altered POM and hence explain the decrease of  $\delta^{13}\text{C}$  with depth in the POM fraction (Jouquet et al. 2016). Yet, the  $\delta^{13}\text{C}$  signals of both Ferralsols showed no notable difference. Therefore, it is more likely, that the more negative values stem from different past vegetation, compared to the other sites. It seems plausible, that the Ferralsols were cultivated as teak plantations before protection of the area as national park, leading to high inputs of depleted root SOC after timber harvest. Conversely, the other sampling sites seems to have experienced a more gradual vegetation shift towards secondary forest. Lastly, the input from deep rooting shrubs such as *L. camara* could also influence the TOC contents and  $\delta^{13}\text{C}$  signals in all soils (Bellè et al. 2022).

### 6.3 Relative importance of stabilisation mechanisms

The relative importance of stabilisation mechanisms might vary with soil type. Ouédraogo et al. (2020) found that the association with oxides, especially short-range-order Fe- and Al-oxides was strongly related to the TC of Lixisols. However, values of Fe and Al were all similarly low for the Lixisols and Ferralsols. Yet, clay content differed and was lower for F1 and F5 as compared to F2 and F6 and the latter two supported higher TOC contents than the former. This suggests that soil texture and the availability of clay mineral surfaces are crucial for SOC stabilisation in heavily weathered soils. Additionally, aggregation of SOC in the surface soil might be influenced by the litter cover, as could be seen in the difference of TOC contents in S+A between Ferralsols and Lixisols.

Vertisols of different parent material stored similar amounts of SOC but of different quality. Clay contents were slightly higher for F4 on amphibolite than F3 on gneiss (see Table 2 Bellè et al. 2022) and so was the TOC concentration of the s+c fraction (see Figure 11), despite a much higher percentage of Fe-oxides in F4. Additionally F4 was dominated by smectite, while F3 contained significant amounts of kaolinite and interlayers kaolinite-smectite (Bellè et al. 2022). Hence available surface area and interaction of clay minerals with oxides might play a more important role than the individual content (Kirsten et al. 2021). Additionally, the presence of carbonates in F3 significantly altered the TOC content and concentration in the S+A fraction and bulk soil. However, SE was large for these samples and  $\delta^{13}\text{C}$  has very high, suggesting improper fumigation treatment.



## 6.4 Methodological limitations

Although trends are visible, fractionation as well as DRIFTS remain qualitative rather than quantitative sources of data. Results are to be interpreted with care, since both methods rely on proxies, assumptions and no direct measurement of the carbon quality is possible. Especially, since fractionation was not developed for tropical but temperate, agricultural soils. Hence, the method has not been tested and optimised for other uses. Findings by Spaccini et al. (2001) further suggest, that DRIFTS is not useful on very sandy or clayey soils. Hence raising the question of the results' validity, since most soils in this thesis fall into either one of those categories. Additionally, fractions should represent non-composite SOC pools, which are functionally different from each other and behave homogeneously with decomposition (Lützow et al. 2007). However, studies found that compounds bind to certain fractions differently under varying climatic conditions (Cates et al. 2022). Further, Curtin et al. (2019) stated that POM is a composite of different organic and mineral materials, rather than a unique fraction and shares characteristics with the silt fraction. Subsequently, if a fraction is not homogeneous, then its stability could differ in varying soils, depending on its specific composition and hence compromising its meaningfulness as model pool (Curtin et al. 2019). However, DRIFTS might provide additional information to support results found through fractionation. This is particularly important, since Poeplau et al. (2013) showed, that fractionation results can vary considerably between different laboratories and are therefore not always reproducible (Poeplau et al. 2013). Yet, DRIFTS measurements have been shown to be sensible to interference from water (Laub et al. 2020; Matamala et al. 2017) and can also be influenced by the degree of milling and laser settings.

Since the available sample quantities were very low for some fractions and samples, the residual water content was not determined and the samples were not dried again before measurement, in order to avoid losing material. Hence, samples likely retained water and regained moisture from ambient air, whenever the storage container was opened (Laub et al. 2020). The accumulated humidity might vary depending on the fraction and the time of processing, for samples were prepared sequentially, starting with sampling site F1. Additionally, the storage containers were not filled to the top, meaning that air exchange would be possible even within an airtight container. Moreover, the less sample, the more air would be in each glass vial. The samples' humidity is important, since the aliphatic carbon band is subject to interference from water. This might dampen the signal and influence the calculated band ratios, which is why Laub et al. (2019) recommended drying samples at 105 °C and keeping them in a desiccator (Laub et al. 2019). However, Demyan et al. 2012 dried samples at only 32 °C and Matamala et al. (2017) found no significant influence on the results, when drying the samples at 65 °C and emphasised that further heating might degrade labile organic compounds, influencing TOC concentration (Matamala et al. 2017). However, no significant impact of water interference could be detected in the DRIFT spectra (see Figure 16).

The importance of DOC in SOC distribution and quality remains unclear and so does the loss of SPT soluble carbon with fractionation. Mass recovery of samples did not always match the respective carbon recovery. Hence carbon was lost during the fractionation process or not measured at all.

Carbon recoveries were generally lower for soils containing more sand, suggesting carbon loss mainly occurred with the S+A fraction, since the s+c fraction has been shown to be the most robust against losses during the fractionation process (Poeplau et al. 2013). This coincides with results from Sollins et al. (2007), who state that the SPT-solubilised carbon fraction might be significant and Plaza et al. (2019) confirm, that SPT density fractionation could result in significant carbon losses from the mineral-associated fraction (Plaza et al. 2019). For this thesis, that would correspond to the S+A fraction, since the s+c fraction was not treated with SPT. This does seem plausible, since the water used for washing out the S+A fraction, did discolour in some cases. However, this form of leaching was not quantified. Nor was the DOC, which could have contained SOC in the form organo-mineral associations with Fe-oxides and clay minerals, since those are on the scale of  $10^{-8}$  to  $10^{-7}$  m. They would have therefore passed the  $0.45\ \mu\text{m}$  filters used in vacuum filtration, since particles in the clay fraction form packages of  $< 20\ \mu\text{m}$  and aggregate to microaggregates ( $20\text{-}250\ \mu\text{m}$ ) which could have been dispersed during sonification (Blume et al. 2016).

## 7 Conclusion

SOC dynamics in the tropics are severely understudied, despite playing a crucial role in the global carbon cycle. Hence this thesis aimed at quantifying SOC composition as well as distribution of carbon pools at the different sampling sites based on fractionation. Further, the goal was to describe carbon quality at the sites based on organic carbon analysis and mid-infrared spectroscopy, and lastly, to propose drivers of differences in SOC quality and distribution.

SOC contents in bulk soil and fractions varied significantly between different soils, with highest values found in the Vertisols. However, soil type was not the main indicator of carbon contents: Parent material, vegetation history and soil texture were instrumental to the stabilisation of SOC. Especially the mineral assemblage explained differences in TOC between soil types, whereas the  $\delta^{13}\text{C}$  was significantly influenced by current and past vegetation cover. The isotopic signal could not have been properly interpreted without additional information on present compounds. DRIFTS offered a low cost and rapid method for compound analysis, bypassing the need for time-intensive extractions of chemical compounds. Although the methodology was not originally developed for tropical soils, measures of carbon recovery showed that it worked fine for most, but not all soils. Samples with high sand contents presented lower carbon recoveries, indicating a significant loss of SOC during the process of fractionation. Hence, I propose to quantify DOC and potentially SPT soluble SOC, in order to increase carbon recovery and present a more complete picture of SOC quality and distribution.

This thesis found that SOC stabilisation and degree of decomposition was proportionally highest in the s+c fraction, followed by S+A and POM. This coincided with finding from most temperate soil studies, although comparison was difficult: Fraction definition and separation methods, SOC terminology, but also general theory of SOC stabilisation vary greatly between studies and do therefore not allow for direct comparison. Especially, since there is a lack of data on the here presented soil types. Tropical, dry deciduous forest soils are subject to strong seasonal variations in litter input and precipitation. They further present unique chemical and physical characteristics, such as shrinking and swelling found in Vertisols or accumulation of oxides in Ferralsols. Therefore, it is crucial to study the influence of these factors on tropical SOC dynamics more thoroughly, in order to better comprehend patterns of SOC quality and distribution and enable tropical soils to be represented properly in global SOC models.

## 8 Outlook

Since tropical soils are underrepresented in global assessments of SOC, the here presented data makes a valuable contribution to the overall understanding of SOC heterogeneity and dynamics (Riotte et al. 2021). Firstly, the meaningfulness of SOC models relies on sufficient and representative data for their initiation and validation (Zimmermann et al. 2007). Moreover, there is a need for studies of SOC at a local and regional scale, which allow to assess and include the diversity of soil types and their specific reactions to climate and land use change (Bellè et al. 2022). Hereby fractionation serve as a useful tool to provide such model proxies. However, it is crucial to challenge results using other methodologies, in order to improve predictions of SOC distribution and quality globally. The here presented DRIFTS data can, in a next step, be further analysed to reveal information about clay mineralogy, oxide contents and more (Calderón et al. 2011). Additionally, SOC fractions and their chemical composition could be analysed together with data collected by Bellè et al. (2022), to find possible correlations with pH or soil texture, among others.

Further, the thermal stability of SOC fractions was analysed using Rock-Eval pyrolysis. However, the data was not ready in time for this thesis, but could give important, additional information on the biochemical stability of the different fractions (Sebag et al. 2016). Other interesting approaches would be the assessment of turnover time, aggregate stability,  $Q_{10}$  or microbial communities, especially over time and during different seasons. However, some unification of methods should be reached, in order to ensure comparability between studies. A first step towards a more integrated approach would be to apply different methods of fractionation to varying tropical soils, in order to identify a best practice. Similar to the review by Poeplau et al. (2018), who finally suggested a combination of particle size and density fractionation after aggregate dispersion and a total of three to five SOC fractions, representing the carbon pools in the most frequently used turnover models, such as RothC (Poeplau et al. 2018). This data may then be additionally evaluated with DRIFTS and possibly Rock-Eval measurements, in order to create a data bank for soil, climate and vegetation specific DRIFT spectra, as proposed by Briedis et al. (2020).

## Bibliography

- Barbiéro, L., M. S. Kumar, A. Violette, P. Oliva, J. J. Braun, C. Kumar, S. Furian, M. Babic, J. Riotte, and V. Valles (2010). “Ferrolisis induced soil transformation by natural drainage in Vertisols of sub-humid South India”. In: *Geoderma* 156.3-4, pp. 173–188.
- Barbiéro, L., H. R. Parate, M. Descloitres, A. Bost, S. Furian, M. S. Mohan Kumar, C. Kumar, and J. J. Braun (2007). “Using a structural approach to identify relationships between soil and erosion in a semi-humid forested area, South India”. In: *Catena* 70.3, pp. 313–329.
- Bellè, S.-L., J. Riotte, M. Sekhar, L. Ruiz, M. Schiedung, and S. Abiven (2022). “Soil organic carbon stocks and quality in small-scale tropical, sub-humid and semi-arid watersheds under shrubland and dry deciduous forest in southwestern India”. In: *Geoderma* 409, p. 115606.
- Blume, H.-P., G. W. Brümmer, H. Fleige, R. Horn, E. Kandeler, I. Kögel-Knabner, R. Kretzschmar, K. Stahr, and B.-M. Wilke (2016). *Scheffer/Schachtschabel Soil Science*. 16th ed. Berlin Heidelberg: Springer Verlag.
- Briedis, C., J. Baldock, J. C. de Moraes Sá, J. B. dos Santos, and D. M. B. P. Milori (2020). “Strategies to improve the prediction of bulk soil and fraction organic carbon in Brazilian samples by using an Australian national mid-infrared spectral library”. In: *Geoderma* 373.114401, pp. 1–13.
- Bruun, T. B., B. Elberling, and B. T. Christensen (2010). “Lability of soil organic carbon in tropical soils with different clay minerals”. In: *Soil Biology and Biochemistry* 42.6, pp. 888–895.
- Buettner, S. W., M. G. Kramer, O. A. Chadwick, and A. Thompson (2014). “Mobilization of colloidal carbon during iron reduction in basaltic soils”. In: *Geoderma* 221-222, pp. 139–145.
- Calderón, F. J., J. B. Reeves, H. P. Collins, and E. A. Paul (2011). “Chemical Differences in Soil Organic Matter Fractions Determined by Diffuse-Reflectance Mid-Infrared Spectroscopy”. In: *Soil Science Society of America Journal* 75.2, pp. 568–579.
- Cates, A. M., A. Jilling, M. M. Tfaily, and R. D. Jackson (2022). “Temperature and moisture alter organic matter composition across soil fractions”. In: *Geoderma* 409.115628, pp. 1–12.
- Chatterjee, S., F. Santos, S. Abiven, B. Itin, R. E. Stark, and J. A. Bird (2012). “Elucidating the chemical structure of pyrogenic organic matter by combining magnetic resonance, mid-infrared spectroscopy and mass spectrometry”. In: *Organic Geochemistry* 51, pp. 35–44.
- Chen, C., S. J. Hall, E. Coward, and A. Thompson (2020). “Iron-mediated organic matter decomposition in humid soils can counteract protection”. In: *Nature Communications* 11.1.
- Christensen, B. T. (2001). “Physical fractionation of soil and structural and functional complexity in organic matter turnover”. In: *European Journal of Soil Science* 52, pp. 345–353.
- Costa, O. Y., J. M. Raaijmakers, and E. E. Kuramae (2018). “Microbial extracellular polymeric substances: Ecological function and impact on soil aggregation”. In: *Frontiers in Microbiology* 9, pp. 1–14.
- Curtin, D., M. H. Beare, W. Qiu, and J. Sharp (2019). “Does Particulate Organic Matter Fraction Meet the Criteria for a Model Soil Organic Matter Pool?” In: *Pedosphere* 29.2, pp. 195–203.
- Demyan, M. S., F. Rasche, E. Schulz, M. Breulmann, T. Müller, and G. Cadisch (2012). “Use of specific peaks obtained by diffuse reflectance Fourier transform mid-infrared spectroscopy to study

- the composition of organic matter in a Haplic Chernozem”. In: *European Journal of Soil Science* 63.2, pp. 189–199.
- FAO (2020). *Global Forest Resources Assessment 2020 - Key findings*. Rome: FAO.
- Filep, T., D. Zacháry, and K. Balog (2016). “Assessment of soil quality of arable soils in Hungary using DRIFT spectroscopy and chemometrics”. In: *Vibrational Spectroscopy* 84, pp. 16–23.
- Ghazoul, J. and D. Sheil (2010). *Tropical rain forest ecology, diversity, and conservation*. New York: Oxford University Press Inc., p. 516.
- Gunina, A. and Y. Kuzyakov (2014). “Pathways of litter C by formation of aggregates and SOM density fractions: Implications from  $^{13}\text{C}$  natural abundance”. In: *Soil Biology and Biochemistry* 71, pp. 95–104.
- Helfrich, M., H. Flessa, R. Mikutta, A. Dreves, and B. Ludwig (2007). “Comparison of chemical fractionation methods for isolating stable soil organic carbon pools”. In: *European Journal of Soil Science* 58.6, pp. 1316–1329.
- IUSS Working Group WRB (2015). *World Reference Base for Soil Resources 2014, update 2015 International soil classification system for naming soils and creating legends for soil maps*. Rome: FAO.
- Jackson, R. B., K. Lajtha, S. E. Crow, G. Hugelius, M. G. Kramer, G. Piñeiro, and P. Piñeiro (2017). “The Ecology of Soil Carbon: Pools, Vulnerabilities, and Biotic and Abiotic Controls”. In: *Annual Review of Ecology, Evolution, and Systematics* 48, pp. 419–464.
- Jindaluang, W., I. Kheoruenromne, A. Suddhiprakarn, B. P. Singh, and B. Singh (2013). “Influence of soil texture and mineralogy on organic matter content and composition in physically separated fractions soils of Thailand”. In: *Geoderma* 195-196, pp. 207–219.
- Jouquet, P., N. Bottinelli, R. R. Shanbhag, T. Bourguignon, S. Traoré, and S. A. Abbasi (2016). “Termites: The neglected soil engineers of tropical soils”. In: *Soil Science* 181.3-4, pp. 157–165.
- Kaiser, K. and G. Guggenberger (2000). “The role of DOM sorption to mineral surfaces in the preservation of organic matter in soils”. In: *Organic Geochemistry* 31, pp. 711–725.
- Kirsten, M., R. Mikutta, C. Vogel, A. Thompson, C. W. Mueller, D. N. Kimaro, H. L. Bergsma, K. H. Feger, and K. Kalbitz (2021). “Iron oxides and aluminous clays selectively control soil carbon storage and stability in the humid tropics”. In: *Scientific Reports* 11.5076, pp. 1–12.
- Kögel-Knabner, I. and W. Amelung (2021). “Soil organic matter in major pedogenic soil groups”. In: *Geoderma* 384.114785, pp. 1–22.
- Laub, M., S. Blagodatsky, Y. F. Nkwain, and G. Cadisch (2019). “Soil sample drying temperature affects specific organic mid-DRIFTS peaks and quality indices”. In: *Geoderma* 355.113897, pp. 1–3.
- Laub, M., M. Scott Demyan, Y. Funkuin Nkwain, S. Blagodatsky, T. Kätterer, H. P. Piepho, and G. Cadisch (2020). “DRIFTS band areas as measured pool size proxy to reduce parameter uncertainty in soil organic matter models”. In: *Biogeosciences* 17.6, pp. 1393–1413.
- Lorenz, K., R. Lal, and J. J. Jiménez (2009). “Soil organic carbon stabilization in dry tropical forests of Costa Rica”. In: *Geoderma* 152.1-2, pp. 95–103.

- Lützw, M. von, I. Kögel-Knabner, K. Ekschmitt, H. Flessa, G. Guggenberger, E. Matzner, and B. Marschner (2007). “SOM fractionation methods: Relevance to functional pools and to stabilization mechanisms”. In: *Soil Biology and Biochemistry* 39.9, pp. 2183–2207.
- Matamala, R., F. J. Calderón, J. D. Jastrow, Z. Fan, S. M. Hofmann, G. J. Michaelson, U. Mishra, and C. L. Ping (2017). “Influence of site and soil properties on the DRIFT spectra of northern cold-region soils”. In: *Geoderma* 305, pp. 80–91.
- Nottingham, A. T., P. Meir, E. Velasquez, and B. L. Turner (2020). “Soil carbon loss by experimental warming in a tropical forest”. In: *Nature* 584, pp. 234–237.
- Ouédraogo, R. A., C. Chartin, F. C. Kambiré, B. van Wesemael, B. Delvaux, H. Milogo, and C. L. Biielders (2020). “Short and long-term impact of urban gardening on soil organic carbon fractions in Lixisols (Burkina Faso)”. In: *Geoderma* 362.114110, pp. 1–11.
- Pal, D. K. (2019). “Organic Carbon Sequestration and Ecosystem Service of Indian Tropical Soils”. In: *Ecosystem Services and Tropical Soils of India*. Cham, Switzerland: Springer Nature Switzerland AG, pp. 29–64.
- Paustian, K., J. Lehmann, S. Ogle, D. Reay, G. P. Robertson, and P. Smith (2016). “Climate-smart soils”. In: *Nature* 532, pp. 49–57.
- Plaza, C., B. Giannetta, I. Benavente, C. Vischetti, and C. Zacccone (2019). “Density-based fractionation of soil organic matter: effects of heavy liquid and heavy fraction washing”. In: *Scientific Reports* 9.10146, pp. 1–7.
- Poeplau, C., A. Don, M. Dondini, J. Leifeld, R. Nemo, J. Schumacher, N. Senapati, and M. Wiesmeier (2013). “Reproducibility of a soil organic carbon fractionation method to derive RothC carbon pools”. In: *European Journal of Soil Science* 64.6, pp. 735–746.
- Poeplau, C., A. Don, J. Six, M. Kaiser, D. Benbi, C. Chenu, M. F. Cotrufo, D. Derrien, P. Gioacchini, S. Grand, E. Gregorich, M. Griepentrog, A. Gunina, M. Haddix, Y. Kuzyakov, A. Kühnel, L. M. Macdonald, J. Soong, S. Trigalet, M. L. Vermeire, P. Rovira, B. van Wesemael, M. Wiesmeier, S. Yeasmin, I. Yevdokimov, and R. Nieder (2018). “Isolating organic carbon fractions with varying turnover rates in temperate agricultural soils – A comprehensive method comparison”. In: *Soil Biology and Biochemistry* 125, pp. 10–26.
- Pulido-Moncada, M., Z. Lozano, M. Delgado, M. Dumon, E. Van Ranst, D. Lobo, D. Gabriels, and W. M. Cornelis (2018). “Using soil organic matter fractions as indicators of soil physical quality”. In: *Soil Use and Management* 34.2, pp. 187–196.
- R Core Team (2020). *R: A language and environment for statistical computing*. Vienna, Austria.
- Riotte, J., J. C. Marechal, S. Audry, C. Kumar, J. P. Bedimo Bedimo, L. Ruiz, M. Sekhar, M. Cisel, R. Chitra Tarak, M. Varma, C. Lagane, P. Reddy, and J. J. Braun (2014). “Vegetation impact on stream chemical fluxes: Mule Hole watershed (South India)”. In: *Geochimica et Cosmochimica Acta* 145, pp. 116–138.
- Riotte, J., J. D. Meunier, T. Zambardi, S. Audry, D. Barboni, K. Anupama, S. Prasad, J. Chmeleff, F. Poitrasson, M. Sekhar, and J. J. Braun (2018). “Processes controlling silicon isotopic fractionation in a forested tropical watershed: Mule Hole Critical Zone Observatory (Southern India)”. In: *Geochimica et Cosmochimica Acta* 228, pp. 301–319.

- Riotte, J., L. Ruiz, S. Audry, B. Baud, J. P. Bedimo Bedimo, L. Boithias, J. J. Braun, B. Dupré, J. L. Duprey, M. Faucheux, C. Lagane, J. C. Marechal, H. Moger, M. S. Mohan Kumar, H. Parate, O. Ribolzi, E. Rochelle-Newall, B. Sriramulu, M. Varma, and M. Sekhar (2021). “The Multiscale TROPICAL CatchmentS critical zone observatory M-TROPICS dataset III: Hydro-geochemical monitoring of the Mule Hole catchment, south India”. In: *Hydrological Processes* 35.5, pp. 1–8.
- Rowley, M. C., S. Grand, and É. P. Verrecchia (2018). “Calcium-mediated stabilisation of soil organic carbon”. In: *Biogeochemistry* 137.1-2, pp. 27–49.
- Rumpel, C. and I. Kögel-Knabner (2011). “Deep soil organic matter—a key but poorly understood component of terrestrial C cycle”. In: *Plant and Soil* 338.1, pp. 143–158.
- Scheinost, A. C. (2005). “Metal oxides”. In: *Encyclopedia of Soils in the Environment*. Ed. by J. L. Hillel Daniel Hatfield. Elsevier Academic Press, pp. 428–438.
- Schmidt, M. W., M. S. Torn, S. Abiven, T. Dittmar, G. Guggenberger, I. A. Janssens, M. Kleber, I. Kögel-Knabner, J. Lehmann, D. A. Manning, P. Nannipieri, D. P. Rasse, S. Weiner, and S. E. Trumbore (2011). “Persistence of soil organic matter as an ecosystem property”. In: *Nature* 478, pp. 49–56.
- Schrumpf, M., K. Kaiser, G. Guggenberger, T. Persson, I. Kögel-Knabner, and E. D. Schulze (2013). “Storage and stability of organic carbon in soils as related to depth, occlusion within aggregates, and attachment to minerals”. In: *Biogeosciences* 10.3, pp. 1675–1691.
- Schulze, D. G. (2005). “Clay minerals”. In: *Encyclopedia of Soils in the Environment*. Ed. by D. Hillel. Elsevier, pp. 246–254.
- Sebag, D., E. P. Verrecchia, L. Cécillon, T. Adatte, R. Albrecht, M. Aubert, F. Bureau, G. Cailleau, Y. Copard, T. Decaens, J. R. Disnar, M. Hetényi, T. Nyilas, and L. Trombino (2016). “Dynamics of soil organic matter based on new Rock-Eval indices”. In: *Geoderma* 284, pp. 185–203.
- Six, J., K. Paustian, E. T. Elliott, and C. Combrink (2000). “Soil Structure and Organic Matter: I. Distribution of Aggregate-Size Classes and Aggregate-Associated Carbon”. In: *Soil Science Society of America Journal* 64, pp. 681–689.
- Sollins, P., C. Swanston, and M. Kramer (2007). “Stabilization and destabilization of soil organic matter - A new focus”. In: *Biogeochemistry* 85, pp. 1–7.
- Spaccini, R., A. Piccolo, G. Haberhauer, M. Stemmer, and M. H. Gerzabek (2001). “Decomposition of maize straw in three European soils as revealed by DRIFT spectra of soil particle fractions”. In: *Geoderma* 99, pp. 245–260.
- Staddon, P. L. (2004). “Carbon isotopes in functional soil ecology”. In: *Trends in Ecology and Evolution* 19.3, pp. 148–154.
- Stahr, K., E. Kandeler, L. Herrmann, and T. Streck (2016). *Bodenkunde und Standortlehre*. 3rd ed. Verlag Eugen Ulmer Stuttgart, p. 320.
- Subashree, K., J. A. Dar, and S. Sundarapandian (2019). “Variation in soil organic carbon stock with forest type in tropical forests of Kanyakumari Wildlife Sanctuary, Western Ghats, India”. In: *Environmental Monitoring and Assessment* 191.690, pp. 1–16.



- Telles Rodrigues, L. A., J. Dieckow, S. Giacomini, A. S. Ottonelli, G. P. Pesenatto Zorzo, and C. Bayer (2022). “Carbon sequestration capacity in no-till soil decreases in the long-term due to saturation of fine silt plus clay-size fraction”. In: *Geoderma* 412.115711, pp. 1–10.
- Toriyama, J., M. Hak, A. Imaya, K. Hirai, and Y. Kiyono (2015). “Effects of forest type and environmental factors on the soil organic carbon pool and its density fractions in a seasonally dry tropical forest”. In: *Forest Ecology and Management* 335, pp. 147–155.
- Walther, L., U. Graf, A. Kammer, J. Luster, D. Pezzotta, S. Zimmermann, and F. Hagedorn (2010). “Determination of organic and inorganic carbon,  $\delta^{13}\text{C}$ , and nitrogen in soils containing carbonates after acid fumigation with HCl”. In: *Journal of Plant Nutrition and Soil Science* 173.2, pp. 207–216.
- Wang, F., Y. Ding, E. J. Sayer, Q. Li, B. Zou, Q. Mo, Y. Li, X. Lu, J. Tang, W. Zhu, and Z. Li (2017). “Tropical forest restoration: Fast resilience of plant biomass contrasts with slow recovery of stable soil C stocks”. In: *Functional Ecology* 31.12, pp. 2344–2355.
- Weil, R. and N. Brady (2017). *The Nature and Properties of Soils*. 15th ed. Pearson Education, p. 1104.
- Wickham, H. (2016). *ggplot2: Elegant Graphics for Data Analysis*. New York: Springer.
- Yeasmin, S., B. Singh, C. T. Johnston, and D. L. Sparks (2017). “Evaluation of pre-treatment procedures for improved interpretation of mid infrared spectra of soil organic matter”. In: *Geoderma* 304, pp. 83–92.
- Yeasmin, S., B. Singh, R. J. Smernik, and C. T. Johnston (2020). “Effect of land use on organic matter composition in density fractions of contrasting soils: A comparative study using  $^{13}\text{C}$  NMR and DRIFT spectroscopy”. In: *Science of the Total Environment* 726.138395, pp. 1–12.
- Zimmermann, M., J. Leifeld, M. W. Schmidt, P. Smith, and J. Fuhrer (2007). “Measured soil organic matter fractions can be related to pools in the RothC model”. In: *European Journal of Soil Science* 58.3, pp. 658–667.

# A Appendix

## A.1 Data overview

### A.1.1 Overview of soil samples and fractionation results

**Table 4:** Overview of the soil samples, their fraction proportion of TOC [%], their mass recovery (M rec) [%] and carbon recovery (C rec) [%]. The fraction proportions were corrected to amount to 100 %. The mass recovery was calculated based on the sum of the mass of the weighed fractions (POM, S+A, s+c) and the initial bulk soil weight. Further, the carbon recovery was calculated based on TC measurements of the fractions as compared to the bulk soil. Lastly, an *r* behind sample names indicates re-fractionation of that sample.

| Sample name | Depth<br>[cm] | Site | M rec<br>[%] | C rec<br>[%] | POM<br>[%] | S+A<br>[%] | s+c<br>[%] |
|-------------|---------------|------|--------------|--------------|------------|------------|------------|
| 246B21LP1   | 0-15          | F1   | 96.83        | 103.62       | 11.20      | 3.81       | 84.99      |
| 246B21LP2   | 0-15          | F1   | 97.06        | 91.29        | 9.50       | 5.81       | 84.69      |
| 246B21LP3   | 0-15          | F1   | 97.54        | 97.24        | 16.65      | 4.53       | 78.82      |
| 246B21LP4   | 0-15          | F2   | 95.59        | 99.28        | 11.84      | 3.05       | 85.11      |
| 246B21LP5   | 0-15          | F2   | 95.87        | 94.63        | 8.66       | 6.28       | 85.06      |
| 246B21LP6   | 0-15          | F2   | 94.35        | 90.53        | 12.44      | 6.01       | 81.55      |
| 246B21LP7   | 0-15          | F3   | 94.39        | 109.53       | 15.50      | 1.32       | 83.18      |
| 246B21LP8   | 0-15          | F3   | 92.61        | 84.31        | 16.80      | 1.31       | 81.89      |
| 246B21LP9   | 0-15          | F3   | 93.82        | 91.80        | 12.83      | 0.88       | 86.29      |
| 246B21LP10r | 0-15          | F4   | 94.94        | 98.98        | 10.77      | 2.81       | 86.42      |
| 246B21LP11r | 0-15          | F4   | 94.92        | 96.59        | 9.17       | 2.34       | 88.49      |
| 246B21LP12r | 0-15          | F4   | 93.30        | 90.44        | 11.20      | 2.41       | 86.39      |
| 246B21LP13  | 0-15          | F5   | 95.34        | 85.87        | 10.75      | 9.06       | 80.19      |
| 246B21LP14  | 0-15          | F5   | 97.64        | 95.28        | 8.67       | 8.28       | 83.04      |
| 246B21LP15  | 0-15          | F5   | 95.17        | 90.47        | 12.02      | 13.35      | 74.63      |
| 246B21LP16  | 0-15          | F6   | 95.70        | 100.17       | 13.91      | 13.16      | 72.93      |
| 246B21LP17  | 0-15          | F6   | 95.28        | 96.36        | 9.33       | 9.97       | 80.70      |
| 246B21LP18  | 0-15          | F6   | 95.65        | 82.75        | 11.25      | 13.77      | 74.98      |
| 246B21LP19  | 15-30         | F1   | 95.39        | 80.06        | 3.04       | 6.43       | 90.53      |
| 246B21LP20  | 15-30         | F1   | 96.18        | 104.62       | 9.91       | 6.22       | 83.87      |
| 246B21LP21  | 15-30         | F1   | 94.45        | 82.89        | 4.35       | 11.29      | 84.36      |
| 246B21LP22  | 15-30         | F2   | 93.57        | 97.84        | 3.55       | 5.90       | 90.56      |
| 246B21LP23  | 15-30         | F2   | 93.75        | 110.19       | 5.96       | 5.54       | 88.50      |
| 246B21LP24  | 15-30         | F2   | 93.01        | 85.41        | 3.26       | 4.98       | 91.76      |
| 246B21LP25  | 15-30         | F3   | 91.82        | 92.13        | 5.14       | 0.86       | 93.99      |
| 246B21LP26  | 15-30         | F3   | 88.14        | 96.43        | 4.31       | 1.28       | 94.41      |

Continued on next page

Table 4 – continued from previous page

| Sample name | Depth<br>[cm] | Site | M rec<br>[%] | C rec<br>[%] | POM<br>[%] | S+A<br>[%] | s+c<br>[%] |
|-------------|---------------|------|--------------|--------------|------------|------------|------------|
| 246B21LP27  | 15-30         | F3   | 87.05        | 102.59       | 3.01       | 1.46       | 95.53      |
| 246B21LP28  | 15-30         | F4   | 89.25        | 92.78        | 4.93       | 3.10       | 91.97      |
| 246B21LP29  | 15-30         | F4   | 89.50        | 93.79        | 2.60       | 3.03       | 94.38      |
| 246B21LP30  | 15-30         | F4   | 88.33        | 106.28       | 3.52       | 2.71       | 93.77      |
| 246B21LP31  | 15-30         | F5   | 94.88        | 106.98       | 2.79       | 5.37       | 91.84      |
| 246B21LP32  | 15-30         | F5   | 95.23        | 115.07       | 3.49       | 6.15       | 90.35      |
| 246B21LP33  | 15-30         | F5   | 94.76        | 101.93       | 3.27       | 3.97       | 92.76      |
| 246B21LP34  | 15-30         | F6   | 91.80        | 98.25        | 2.66       | 5.00       | 92.34      |
| 246B21LP35  | 15-30         | F6   | 91.48        | 102.47       | 1.65       | 3.96       | 94.40      |
| 246B21LP36  | 15-30         | F6   | 93.95        | 82.97        | 3.13       | 5.89       | 90.98      |
| 246B21LP37  | 30-45         | F1   | 91.29        | 81.19        | 1.72       | 7.82       | 90.46      |
| 246B21LP38  | 30-45         | F1   | 92.74        | 79.08        | 5.06       | 9.42       | 85.52      |
| 246B21LP39r | 30-45         | F1   | 89.01        | 83.95        | 9.27       | 8.86       | 81.87      |
| 246B21LP40  | 30-45         | F2   | 90.07        | 81.46        | 3.61       | 10.36      | 86.03      |
| 246B21LP41  | 30-45         | F2   | 92.72        | 86.82        | 3.77       | 7.21       | 89.02      |
| 246B21LP42  | 30-45         | F2   | 93.30        | 80.69        | 2.21       | 11.81      | 85.98      |
| 246B21LP43  | 30-45         | F3   | 93.93        | 86.25        | 2.42       | 35.16      | 62.42      |
| 246B21LP44r | 30-45         | F3   | 90.91        | 97.84        | 7.60       | 1.44       | 90.97      |
| 246B21LP45r | 30-45         | F3   | 85.49        | 92.35        | 7.65       | 1.38       | 90.97      |
| 246B21LP46  | 30-45         | F4   | 88.29        | 86.18        | 1.45       | 2.66       | 95.89      |
| 246B21LP47  | 30-45         | F4   | 88.64        | 86.90        | 2.30       | 3.74       | 93.97      |
| 246B21LP48r | 30-45         | F4   | 87.02        | 89.20        | 4.93       | 3.46       | 91.61      |
| 246B21LP49  | 30-45         | F5   | 93.23        | 100.18       | 5.60       | 6.46       | 87.94      |
| 246B21LP50r | 30-45         | F5   | 93.29        | 73.99        | 5.37       | 15.10      | 79.53      |
| 246B21LP51  | 30-45         | F5   | 92.71        | 92.01        | 3.47       | 4.69       | 91.84      |
| 246B21LP52  | 30-45         | F6   | 89.61        | 97.30        | 5.63       | 6.00       | 88.37      |
| 246B21LP53  | 30-45         | F6   | 89.02        | 90.79        | 2.03       | 6.78       | 91.19      |
| 246B21LP54r | 30-45         | F6   | 85.71        | 79.05        | 5.00       | 7.39       | 87.61      |
| 246B21LP55r | 45-60         | F1   | 86.33        | 64.09        | 7.99       | 9.58       | 82.43      |
| 246B21LP56r | 45-60         | F1   | 85.61        | 78.00        | 11.02      | 9.20       | 79.78      |
| 246B21LP57r | 45-60         | F1   | 84.37        | 68.84        | 6.31       | 8.91       | 84.79      |
| 246B21LP58  | 45-60         | F2   | 92.23        | 81.88        | 1.29       | 12.75      | 85.96      |
| 246B21LP59  | 45-60         | F2   | 88.84        | 82.96        | 6.28       | 15.22      | 78.50      |
| 246B21LP60  | 45-60         | F2   | 87.48        | 77.61        | 2.24       | 16.48      | 81.29      |

Continued on next page

**Table 4 – continued from previous page**

| Sample name | Depth<br>[cm] | Site | M rec<br>[%] | C rec<br>[%] | POM<br>[%] | S+A<br>[%] | s+c<br>[%] |
|-------------|---------------|------|--------------|--------------|------------|------------|------------|
| 246B21LP61  | 45-60         | F3   | 94.44        | 95.78        | 2.69       | 43.07      | 54.24      |
| 246B21LP62  | 45-60         | F3   | 96.46        | 99.92        | 2.62       | 53.63      | 43.76      |
| 246B21LP63  | 45-60         | F3   | 93.58        | 90.10        | 5.72       | 27.98      | 66.29      |
| 246B21LP64r | 45-60         | F4   | 85.44        | 89.11        | 7.17       | 2.97       | 89.87      |
| 246B21LP65  | 45-60         | F4   | 87.75        | 85.61        | 7.23       | 10.60      | 82.17      |
| 246B21LP66  | 45-60         | F4   | 87.57        | 86.66        | 5.02       | 3.01       | 91.97      |
| 246B21LP67  | 45-60         | F5   | 91.08        | 79.80        | 9.90       | 12.33      | 77.77      |
| 246B21LP68r | 45-60         | F5   | 88.29        | 72.20        | 11.13      | 9.48       | 79.39      |
| 246B21LP69  | 45-60         | F5   | 89.40        | 75.48        | 7.68       | 14.36      | 77.96      |
| 246B21LP70  | 45-60         | F6   | 86.56        | 90.02        | 2.40       | 5.61       | 91.99      |
| 246B21LP71  | 45-60         | F6   | 86.68        | 92.40        | 5.56       | 6.89       | 87.55      |
| 246B21LP72r | 45-60         | F6   | 87.87        | 75.24        | 6.81       | 8.15       | 85.03      |

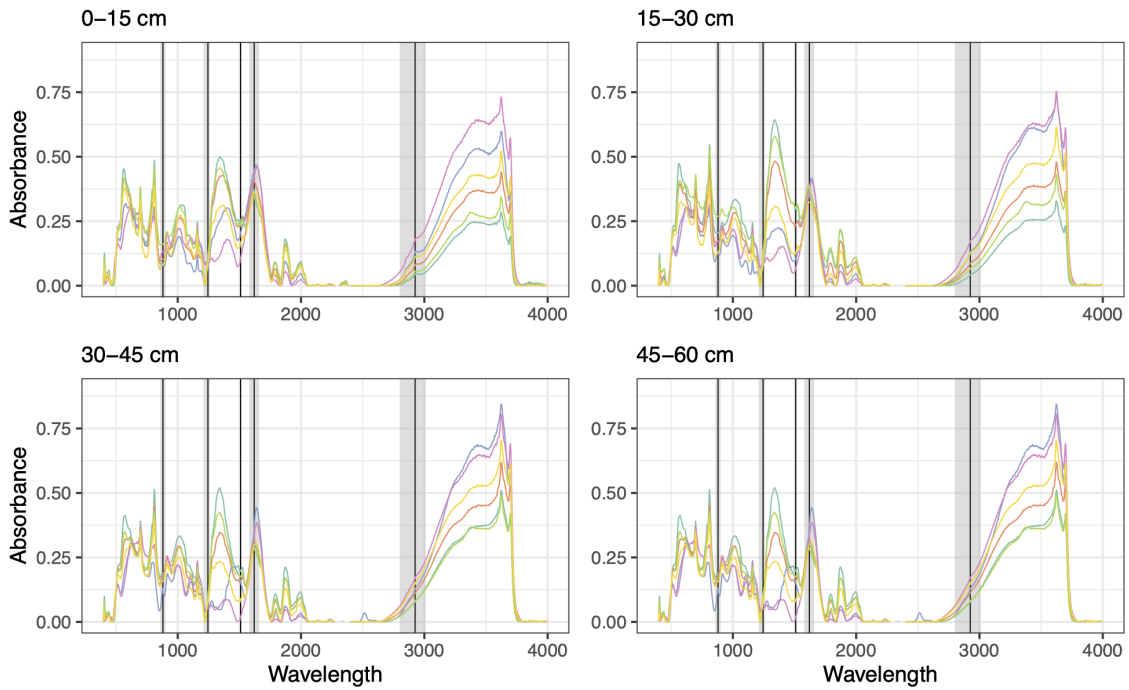
**Table 5:** TC [%], TOC [%] and respective  $\delta^{13}\text{C}$  measurements for the carbon fractions. Values represent the mean by sampling site and depth (n = 3) and the SE is denoted in parentheses. Measurements of the bulk soil can be found in section 5.

| Site | Depth<br>[cm] | Bulk soil   |                |             |                 | POM          |                |              |                 | S+A         |                |             |                 | s+c         |                |             |                 |
|------|---------------|-------------|----------------|-------------|-----------------|--------------|----------------|--------------|-----------------|-------------|----------------|-------------|-----------------|-------------|----------------|-------------|-----------------|
|      |               | TC<br>[%]   | TC_d13C<br>[‰] | TOC<br>[%]  | TOC_d13C<br>[‰] | TC<br>[%]    | TC_d13C<br>[‰] | TOC<br>[%]   | TOC_d13C<br>[‰] | TC<br>[%]   | TC_d13C<br>[‰] | TOC<br>[%]  | TOC_d13C<br>[‰] | TC<br>[%]   | TC_d13C<br>[‰] | TOC<br>[%]  | TOC_d13C<br>[‰] |
| F1   | 0-15          | 2.02 (0.04) | -27.04 (0.51)  | 2.18 (0.07) | -26.62 (0.34)   | 25.10 (2.46) | -29.03 (0.23)  | 26.21 (2.31) | -29.00 (0.52)   | 0.15 (0.02) | -29.42 (0.69)  | 0.17 (0.01) | -30.61 (0.85)   | 4.53 (0.13) | -26.35 (0.54)  | 5.02 (0.17) | -26.84 (0.39)   |
|      | 15-30         | 0.77 (0.06) | -23.67 (0.29)  | 0.81 (0.04) | -23.07 (0.12)   | 25.49 (3.82) | -28.72 (0.08)  | 25.63 (4.14) | -28.72 (0.15)   | 0.06 (0.01) | -29.37 (1.02)  | 0.08 (0.00) | -26.65 (0.91)   | 1.80 (0.17) | -24.34 (0.23)  | 1.70 (0.18) | -24.01 (0.01)   |
|      | 30-45         | 0.49 (0.06) | -23.31 (0.05)  | 0.54 (0.03) | -23.70 (0.16)   | 15.92 (5.81) | -28.85 (0.06)  | 14.02 (5.27) | -27.87 (0.65)   | 0.05 (0.01) | -26.22 (2.24)  | 0.08 (0.01) | -26.62 (0.69)   | 1.01 (0.13) | -23.15 (0.70)  | 1.26 (0.05) | -23.48 (0.47)   |
|      | 45-60         | 0.46 (0.04) | -23.53 (0.35)  | 0.49 (0.02) | -22.79 (0.20)   | 11.27 (1.72) | -28.63 (0.31)  | 11.00 (1.76) | -28.69 (0.28)   | 0.05 (0.01) | -21.63 (1.02)  | 0.07 (0.01) | -24.89 (0.82)   | 0.70 (0.07) | -20.96 (0.19)  | 0.86 (0.08) | -21.95 (0.14)   |
| F2   | 0-15          | 2.95 (0.10) | -27.34 (0.47)  | 3.15 (0.11) | -26.89 (0.31)   | 34.18 (1.05) | -29.99 (0.58)  | 33.57 (1.06) | -30.40 (0.50)   | 0.28 (0.05) | -30.43 (1.48)  | 0.27 (0.04) | -31.09 (1.52)   | 5.47 (0.38) | -26.46 (0.32)  | 5.40 (0.39) | -27.05 (0.48)   |
|      | 15-30         | 1.68 (0.08) | -25.35 (0.23)  | 1.78 (0.09) | -24.91 (0.13)   | 37.33 (3.82) | -29.26 (0.22)  | 34.05 (1.62) | -29.77 (0.23)   | 0.11 (0.01) | -30.23 (0.95)  | 0.13 (0.01) | -28.11 (0.87)   | 3.62 (0.16) | -24.99 (0.21)  | 2.65 (0.16) | -25.85 (0.15)   |
|      | 30-45         | 1.00 (0.11) | -23.63 (0.36)  | 0.99 (0.06) | -23.91 (0.20)   | 32.75 (1.82) | -28.77 (0.35)  | 32.18 (2.30) | -28.45 (0.06)   | 0.10 (0.01) | -26.64 (1.13)  | 0.13 (0.01) | -25.80 (1.20)   | 1.92 (0.19) | -24.46 (0.30)  | 1.54 (0.15) | -24.91 (0.32)   |
|      | 45-60         | 0.67 (0.03) | -22.87 (0.28)  | 0.77 (0.01) | -22.32 (0.20)   | 28.38 (4.89) | -29.15 (0.32)  | 29.53 (6.32) | -28.73 (0.29)   | 0.12 (0.01) | -19.62 (1.12)  | 0.14 (0.01) | -19.87 (1.08)   | 1.18 (0.05) | -23.12 (0.13)  | 0.98 (0.05) | -23.06 (0.19)   |
| F3   | 0-15          | 4.80 (0.38) | -28.99 (0.08)  | 4.49 (0.18) | -28.46 (0.10)   | 36.04 (0.21) | -30.69 (0.10)  | 36.77 (0.55) | -30.85 (0.19)   | 0.14 (0.01) | -30.84 (0.28)  | 0.14 (0.01) | -32.21 (0.35)   | 6.43 (0.07) | -27.33 (0.33)  | 5.36 (0.36) | -28.54 (0.33)   |
|      | 15-30         | 2.01 (0.12) | -25.75 (0.41)  | 1.80 (0.09) | -25.94 (0.21)   | 31.80 (3.13) | -29.71 (0.20)  | 32.74 (1.99) | -29.49 (0.52)   | 0.08 (0.03) | -27.76 (0.69)  | 0.09 (0.03) | -31.02 (1.50)   | 3.05 (0.18) | -25.57 (0.40)  | 2.83 (0.37) | -26.25 (0.11)   |
|      | 30-45         | 1.53 (0.30) | -21.35 (1.47)  | 1.05 (0.02) | -24.20 (0.23)   | 34.23 (1.37) | -29.61 (0.15)  | 32.35 (1.79) | -29.69 (0.22)   | 0.84 (0.60) | -17.50 (5.12)  | 0.63 (0.54) | -24.33 (6.36)   | 1.61 (0.13) | -22.47 (0.78)  | 1.51 (0.05) | -24.16 (0.66)   |
|      | 45-60         | 2.10 (0.29) | -16.20 (1.05)  | 0.91 (0.05) | -22.72 (0.45)   | 27.60 (2.38) | -30.45 (0.85)  | 27.86 (1.05) | -30.34 (0.38)   | 2.95 (0.44) | -10.38 (0.75)  | 2.04 (0.46) | -10.26 (0.91)   | 1.73 (0.45) | -20.24 (1.12)  | 1.13 (0.08) | -23.47 (0.25)   |
| F4   | 0-15          | 4.86 (0.03) | -26.14 (0.42)  | 4.16 (0.16) | -25.53 (0.22)   | 36.30 (0.49) | -26.66 (0.46)  | 35.68 (1.31) | -26.80 (0.29)   | 0.45 (0.04) | -25.98 (0.42)  | 0.46 (0.03) | -25.91 (0.33)   | 5.90 (0.15) | -24.31 (0.37)  | 5.63 (0.13) | -24.87 (0.34)   |
|      | 15-30         | 2.83 (0.14) | -24.06 (0.56)  | 2.63 (0.10) | -24.91 (0.34)   | 41.58 (3.30) | -27.64 (0.69)  | 40.89 (0.54) | -27.00 (0.55)   | 0.22 (0.01) | -26.18 (0.96)  | 0.24 (0.01) | -25.25 (0.83)   | 4.11 (0.14) | -24.39 (0.57)  | 2.97 (0.14) | -25.11 (0.43)   |
|      | 30-45         | 2.18 (0.10) | -22.70 (0.48)  | 1.94 (0.09) | -23.84 (0.31)   | 32.79 (5.16) | -25.63 (0.60)  | 31.34 (3.71) | -25.98 (1.03)   | 0.18 (0.02) | -24.78 (0.30)  | 0.22 (0.04) | -24.15 (0.91)   | 2.86 (0.10) | -23.48 (0.32)  | 2.44 (0.23) | -23.87 (0.27)   |
|      | 45-60         | 1.77 (0.08) | -21.91 (0.34)  | 1.66 (0.01) | -22.35 (0.20)   | 31.22 (4.75) | -26.39 (1.52)  | 30.91 (4.17) | -25.47 (1.26)   | 0.22 (0.05) | -19.75 (1.86)  | 0.24 (0.05) | -20.16 (1.91)   | 2.44 (0.01) | -22.27 (0.55)  | 2.38 (0.06) | -22.56 (0.31)   |
| F5   | 0-15          | 2.00 (0.19) | -28.09 (0.14)  | 1.74 (0.10) | -26.66 (0.23)   | 32.65 (0.46) | -29.07 (0.37)  | 32.15 (0.31) | -29.15 (0.33)   | 0.26 (0.03) | -30.41 (0.70)  | 0.33 (0.02) | -30.02 (0.26)   | 3.29 (0.38) | -26.51 (0.51)  | 2.89 (0.44) | -25.92 (0.47)   |
|      | 15-30         | 0.95 (0.12) | -25.35 (0.28)  | 0.89 (0.10) | -25.01 (0.23)   | 24.02 (2.09) | -28.04 (0.36)  | 24.08 (2.36) | -27.75 (0.22)   | 0.10 (0.02) | -30.42 (2.35)  | 0.12 (0.02) | -31.71 (1.36)   | 1.99 (0.37) | -25.59 (0.80)  | 1.95 (0.30) | -25.42 (0.29)   |
|      | 30-45         | 0.74 (0.11) | -25.07 (0.30)  | 0.70 (0.06) | -24.81 (0.19)   | 27.10 (3.86) | -28.19 (0.63)  | 27.85 (4.83) | -27.81 (0.63)   | 0.08 (0.01) | -25.08 (2.43)  | 0.11 (0.02) | -25.33 (1.59)   | 1.36 (0.28) | -24.23 (0.86)  | 1.33 (0.23) | -24.46 (0.75)   |
|      | 45-60         | 0.59 (0.07) | -25.12 (0.39)  | 0.62 (0.04) | -25.00 (0.40)   | 25.99 (2.75) | -28.93 (0.24)  | 25.62 (2.03) | -28.39 (0.15)   | 0.10 (0.01) | -18.86 (0.64)  | 0.13 (0.01) | -20.25 (0.47)   | 0.84 (0.11) | -24.75 (1.48)  | 0.94 (0.10) | -23.69 (0.72)   |
| F6   | 0-15          | 3.27 (0.12) | -26.90 (0.28)  | 3.15 (0.08) | -26.20 (0.29)   | 34.34 (1.32) | -29.41 (0.17)  | 32.82 (2.04) | -28.90 (0.33)   | 0.51 (0.01) | -28.05 (0.14)  | 0.62 (0.05) | -27.67 (0.17)   | 4.95 (0.06) | -25.85 (0.60)  | 3.35 (0.51) | -26.58 (0.24)   |
|      | 15-30         | 1.84 (0.04) | -24.87 (0.12)  | 1.75 (0.05) | -25.07 (0.21)   | 33.74 (2.21) | -28.47 (0.18)  | 31.80 (2.56) | -27.70 (0.10)   | 0.15 (0.01) | -28.55 (0.53)  | 0.18 (0.01) | -27.82 (0.36)   | 3.10 (0.12) | -24.57 (0.20)  | 2.62 (0.15) | -25.33 (0.20)   |
|      | 30-45         | 1.36 (0.09) | -24.72 (0.64)  | 1.25 (0.05) | -24.97 (0.38)   | 26.79 (5.45) | -28.11 (0.26)  | 26.87 (5.84) | -28.10 (0.22)   | 0.14 (0.01) | -25.86 (2.62)  | 0.18 (0.01) | -26.12 (0.99)   | 2.20 (0.17) | -24.56 (0.72)  | 1.70 (0.09) | -25.01 (0.71)   |
|      | 45-60         | 1.26 (0.09) | -24.40 (0.39)  | 1.32 (0.05) | -24.50 (0.25)   | 28.80 (1.93) | -29.19 (0.66)  | 28.16 (2.35) | -28.58 (0.10)   | 0.14 (0.02) | -23.69 (0.72)  | 0.15 (0.01) | -24.19 (0.47)   | 2.10 (0.02) | -23.90 (0.66)  | 1.73 (0.09) | -24.33 (0.45)   |

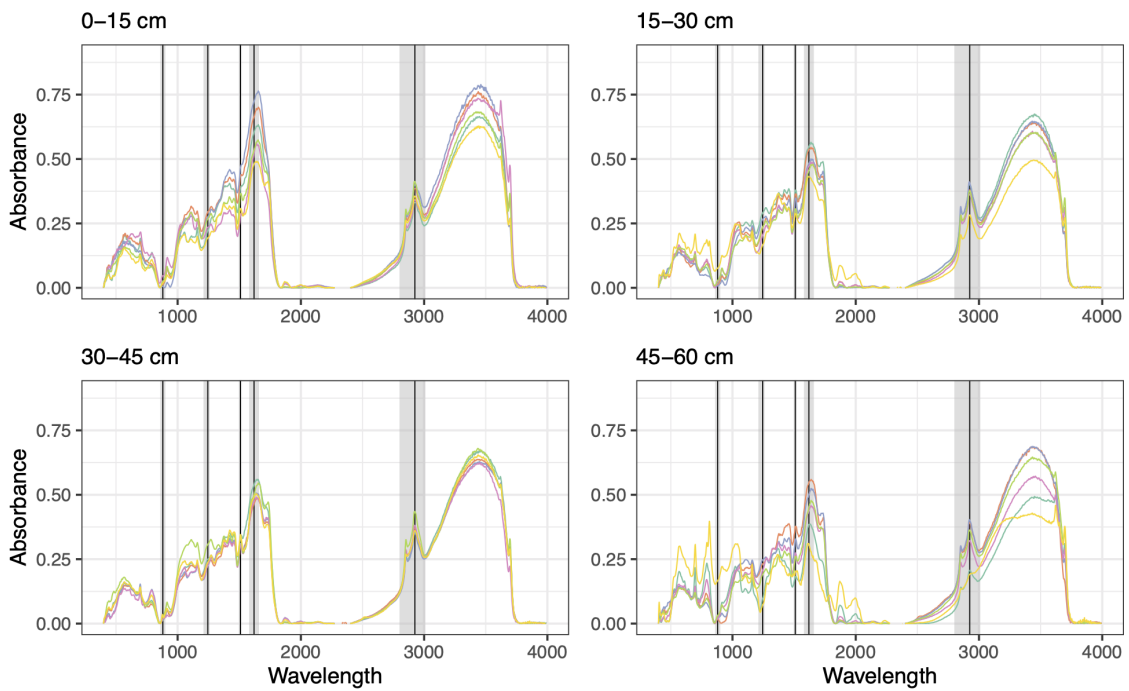
### A.1.2 Checking peaks in the DRIFT spectra

The grey bands in Figures 16 and 17 indicate the integration range and the vertical, black lines the wavelength [ $\text{cm}^{-1}$ ], where peaks are most common: 880, 1245, 1510, 1620 and 2925  $\text{cm}^{-1}$ . These correspond to the aromatic, cellulose, lignin, aromatic and aliphatic carbon bands respectively. The peaks generally fell within the range of integration, although not all fractions showed visible peaks at the points of interest. For example cellulose could only really be detected within the POM fraction and was otherwise only visible in for the Vertisols. Further, the aromatic carbon peaks at 1620  $\text{cm}^{-1}$  were slightly shifted to the right for Vertisols in the bulk fraction and for all soil within the POM fraction. Moreover, signals for aliphatic carbon were very low for the S+A fraction but comparatively high for the aromatic carbon at 880  $\text{cm}^{-1}$ . Notably, the s+c fractions showed high peaks between 3500-3750  $\text{cm}^{-1}$ , which can be attributed to the presence of oxides (Filep et al. 2016) and POM had a high, broad band at 3400  $\text{cm}^{-1}$ , which is due to OH or NH stretching and typical plant residues (Calderón et al. 2011). Therefore, F4 seemed to contain higher levels of plant residues in the S+A fraction at 0-15  $\text{cm}^{-1}$  and F6 and higher amount of oxides at 45-60  $\text{cm}^{-1}$ . Lastly, there is little noise caused by water interference in the band areas above 3000  $\text{cm}^{-1}$ .

## Bulk soil



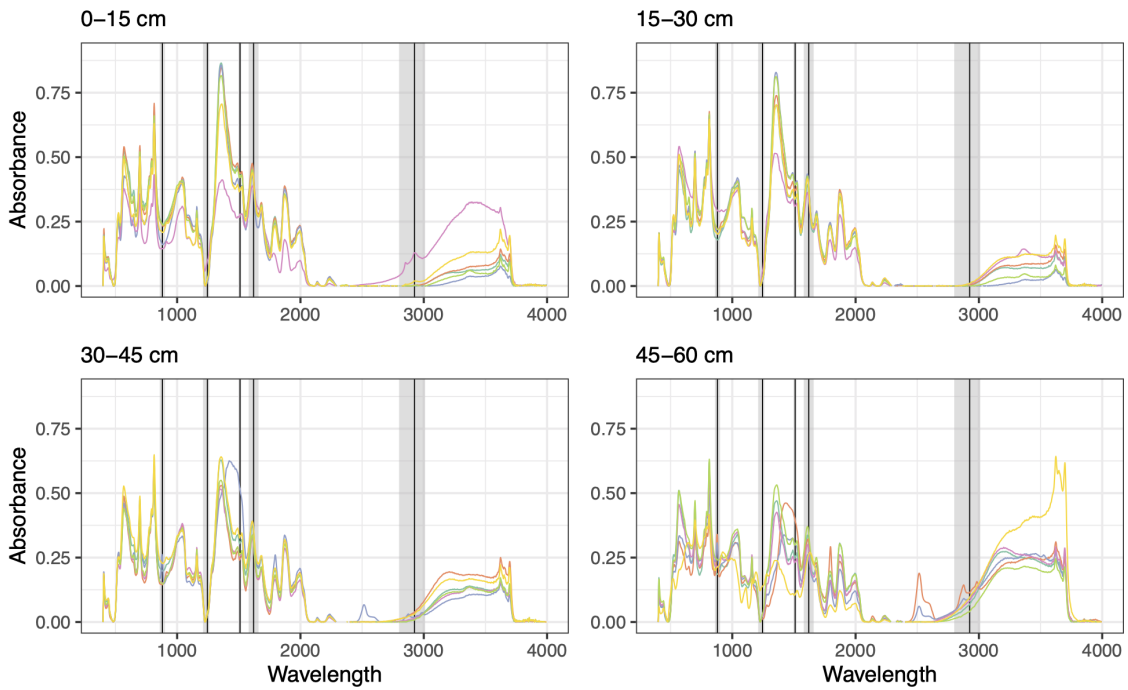
## Particulate organic matter



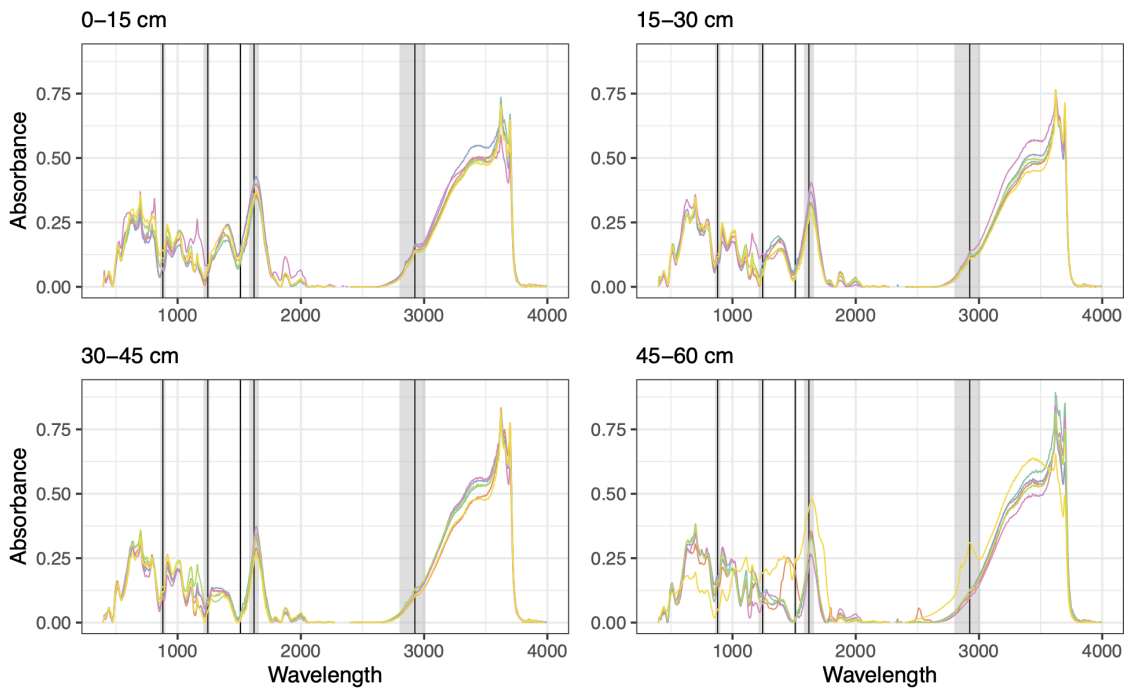
Sampling site — F1 — F3 — F5  
— F2 — F4 — F6

**Figure 16:** DRIFT spectra of the bulk soil and POM fraction. Values represent the mean ( $n = 3$ ) of DRIFT spectra obtained per fraction, sampling site and depth (POM, F2, 45-60 cm:  $n = 2$ ).

## Sand and aggregates



## Silt and clay



Sampling site F1 F3 F5  
F2 F4 F6

**Figure 17:** DRIFT spectra of the S+A and s+c fraction. Values represent the mean ( $n = 3$ ) of DRIFT spectra obtained per fraction, sampling site and depth.



## A.2 Data processing and visualisation with R

### A.2.1 Statistical testing of total organic carbon

For Figure 11, the TOC [g C kg<sup>-1</sup> soil] measurements were subset by depth and fraction in order to allow for comparison between sampling sites as independent variables. The data subsets were tested for normal distribution (Shapiro-Wilk test) and for the equality of variance (Levene's test) before performing a one-way ANOVA and post hoc Tukey's test for pairwise comparison. Further, residuals were tested for normality with Shapiro-Wilk. Some data subsets were transformed to meet the assumption of normality (see Table 6) and the bulk soil at 45-60 cm was excluded from the model, since it was not normally distributed (see Figure 20). Hence, Kruskal-Wallis and pairwise Wilcoxon rank sum test were applied as non-parametric tests (see Table 8). Additionally, some outliers were removed in the S+A fraction of site F3, which corresponded to the calcite-containing depths and are visible in Figure 18. Last, Figure 19 shows the residuals of the ANOVA performed for S+A at 0-15 cm, which were not normally distributed.

**Table 6:** Overview of data transformations of TOC [g C kg<sup>-1</sup> soil].

| Fraction | Depth [cm] | Transformation |
|----------|------------|----------------|
| bulk     | 30-45      | sqrt()         |
| s+c      | 45-60      | sqrt()         |
| POM      | 0-15       | 1/x            |
| POM      | 15-30      | log            |
| POM      | 30-45      | sqrt()         |
| POM      | 45-60      | sqrt()         |

**Table 7:** P-values of the statistical tests applied to the TOC data. P-values  $\leq 0.05$  are denoted in italic font.

| Fraction | p-values  | 0-15 cm      | 15-30 cm | 30-45 cm | 45-60 cm |
|----------|-----------|--------------|----------|----------|----------|
| bulk     | shapiro   | 0.143        | 0.083    | 0.102    |          |
|          | levne     | 0.235        | 0.114    | 0.170    | 0.191    |
|          | residuals | 0.807        | 0.579    | 0.537    |          |
| POM      | shapiro   | 0.053        | 0.103    | 0.729    | 0.271    |
|          | levne     | 0.726        | 0.743    | 0.317    | 0.475    |
|          | residuals | 0.083        | 0.899    | 0.649    | 0.594    |
| S+A      | shapiro   | 0.154        | 0.275    | 0.255    | 0.097    |
|          | levne     | 0.554        | 0.593    | 0.284    | 0.720    |
|          | residuals | <i>0.027</i> | 0.480    | 0.091    | 0.153    |
| s+c      | shapiro   | 0.096        | 0.713    | 0.055    | 0.067    |
|          | levne     | 0.816        | 0.570    | 0.629    | 0.489    |
|          | residuals | 0.769        | 0.814    | 0.824    | 0.448    |

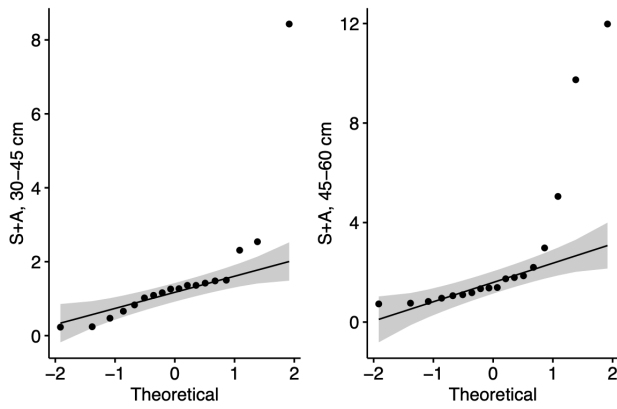


**Figure 18:** QQ-plots of F3 at 30-45 cm and 45-60 cm for the S+A fraction. Outliers corresponded to samples number 246B21LP43 as well as 246B21LP61-246B21LP63r respectively and were removed.

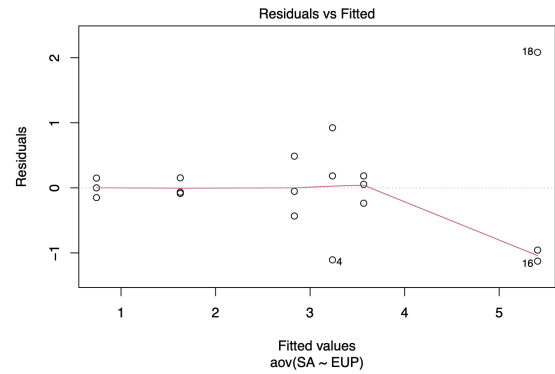


**Figure 19:** Residuals of the ANOVA on the S+A fraction for the first depth interval, 0-15 cm. Outlier 4 corresponds to sampling site F2 and, 16 and 18 correspond to F6.

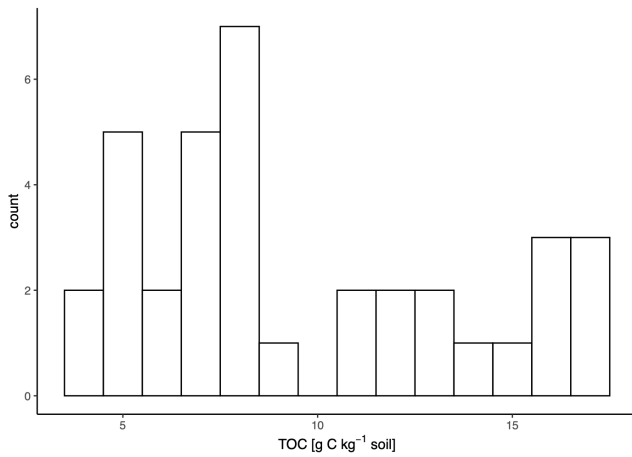


**Figure 20:** Histogram of the bulk soil data subset of TOC [g C kg<sup>-1</sup> soil] at 45-60 cm.

**Table 8:** Overview of the pairwise Wilcoxon rank sum test results for TOC [g C kg<sup>-1</sup> soil] between sampling sites (F1-F6) of the bulks soil at 45-60 cm. All soil are significantly different from each other, except F1 and F5 ( $p > 0.05$ ).

|    | F1     | F2     | F3     | F4     | F5     |
|----|--------|--------|--------|--------|--------|
| F2 | 0.0027 | -      | -      | -      | -      |
| F3 | 0.0027 | 0.0093 | -      | -      | -      |
| F4 | 0.0027 | 0.0027 | 0.0027 | -      | -      |
| F5 | 0.0649 | 0.005  | 0.0027 | 0.0027 | -      |
| F6 | 0.0027 | 0.0027 | 0.0027 | 0.0027 | 0.0027 |

## A.2.2 Calculating significance levels

```
##### set up #####

rm(list = ls()) #reset environment
setwd() #set working directory
dat <- read.csv("TOC.csv", sep = ";", header = T) #load data
dat$depth <- as.factor(dat$depth)
dat$EUP <- as.factor(dat$EUP)

p <- list() #create list to store plots

### load relevant packages ###
library(ggplot2)
library(multcompView)
library(dplyr)
library(tidyr)
library(pgirmess)
library(patchwork)
library(car)
library(moments)
library(ggpubr)
library(gridExtra)

##### bulk soil #####

#subset bulk data
sub_bulk <- dat[,c(1:4, 18, 19)]
#convert to long data
sub_bulk_l <- gather(sub_bulk, fraction, bulk, bulk_mg_g_1:bulk_mg_g_2, factor_key=TRUE)
#subset by depth
subA <- sub_bulk_l[which(sub_bulk_l$depth == "0-15"), c(1:3,6)]
subB <- sub_bulk_l[which(sub_bulk_l$depth == "15-30"), c(1:3,6)]
subC <- sub_bulk_l[which(sub_bulk_l$depth == "30-45"), c(1:3,6)]
subD <- sub_bulk_l[which(sub_bulk_l$depth == "45-60"), c(1:3,6)]

### test subsets ###

#homogeneity of variance
leveneTest(bulk ~ EUP, data = subA)
leveneTest(bulk ~ EUP, data = subB)
leveneTest(bulk ~ EUP, data = subC)
leveneTest(bulk ~ EUP, data = subD)
#normality
shapiro.test(subA$bulk)
shapiro.test(subB$bulk)
shapiro.test(subC$bulk) #no normal distribution -> transform
shapiro.test(subD$bulk) #no normal distribution -> transformation not possible

#check and visualise
skewness(subC$bulk) #positively skewed
skewness(subD$bulk) #positively skewed
ggqqplot(subC$bulk, ylab = "bulk soil, 30-45 cm")
ggqqplot(subD$bulk, ylab = "bulk soil, 45-60 cm")

#transform w/ sqrt()
subC$bulk_sqrt <- sqrt(subC$bulk)

#recheck
shapiro.test(subC$bulk_sqrt)

#find outliers
hist(subD$bulk, main = "", xlab = "Bulk soil, 45-60 cm") #non-parametric test necessary
```

**Figure 21:** Code used to calculate significance levels by depth, as is shown in Figure 11. Only the code for bulk soil is shown. However, all other fractions were computed in the same way. Continued on next page.

```

### create labels of significance values ###

#0-15 cm
anovaA <- aov(bulk ~ EUP, data = subA)           #run ANOVA
tukeyA <- TukeyHSD(anovaA, conf.level = 0.95)    #run Tukey pairwise comparison on ANOVA
cldA <- multcompLetters4(anovaA, tukeyA)        #create letter labels based on tukey

dtA <- group_by(subA, EUP) %>%                  #compute summary statistics of data subset
  summarise(N = length(bulk), w = mean(bulk), sd = sd(bulk), se = sd / sqrt(N))%>%
  arrange(desc(w))

cldA <- as.data.frame.list(cldA$EUP)           #save labels as df
dtA$cldA <- cldA$Letters                       #add to statistics
dtA$depth <- as.factor("0-15")

##### repeat for other depth subsets #####

### test residuals ###

shapiro.test(x = residuals(object = anovaA))
shapiro.test(x = residuals(object = anovaB))
shapiro.test(x = residuals(object = anovaC))

### plot ###

#statistics of the entire fraction data set
bulk_stats <- sub_bulk_1%>%
  group_by(depth, EUP) %>%
  summarise(N = length(bulk), w = mean(bulk), sd = sd(bulk), se = sd / sqrt(N)) %>%
  arrange(desc(w))
print(bulk_stats)

#combine labels of all subsets
labels <- rbind(dtA, dtB, dtC)                 #no labels for 45-60cm

#add labels to stats
bulk_stats <- merge(labels,bulk_stats,by=c("EUP","depth", "w", "sd", "se", "N"), all = TRUE)

#plot
pbulk <- ggplot(bulk_stats, aes(x = EUP, y = w)) + ggtitle("Bulk soil")+
  geom_bar(stat = 'identity', fill = "lightgrey") + facet_grid(~ depth) +
  geom_errorbar(aes(ymin = w-se, ymax = w+se), width = .4) +
  ylab(expression(paste("TOC [g C ", kg^-1, " soil]"))) + xlab("Sampling site") +
  theme_classic() + geom_text(aes(label = label, y = w+se+1.5)) + ylim(0,50)

```

Figure 21: Continued from previous page.

## A.2.3 Plotting of TOC and $\delta^{13}\text{C}$

```
##### set up #####

rm(list = ls()) #reset environment
setwd() #set working directory
dat <- read.csv("TOC.csv", sep = ";", header = T) #load data
dat$depth <- as.factor(dat$depth)
dat$EUP <- as.factor(dat$EUP)

### load relevant packages ###
library(tidyr)
library(ggplot2)
library(rstatix)
library(ggpubr)
library(plyr)
library(dplyr)
library(conflicted)
conflict_prefer("filter", "dplyr") # filter can be used without dplyr
conflict_prefer("mutate", "dplyr") # filter can be used without dplyr
conflict_prefer("rename", "dplyr") # filter can be used without dplyr
conflict_prefer("summarize", "plyr") # filter can be used without dplyr
conflict_prefer("summarise", "dplyr")
library(multcompView)
library(rcompanion)
library(moments)
library(patchwork)

##### bulk soil #####

### same process for delta 13C and TOC ###
#subset by sampling site
sub_EUP56_d <- dat_delta[ which(dat_delta$EUP=="F1" | dat_delta$EUP=="F2"), c(1:5)]
sub_EUP78_d <- dat_delta[ which(dat_delta$EUP=="F3" | dat_delta$EUP=="F4"), c(1:5)]
sub_EUP910_d <- dat_delta[ which(dat_delta$EUP=="F5" | dat_delta$EUP=="F6"), c(1:5)]
#reshape to long data
sub_EUP56_d_l <- gather(sub_EUP56_d, fraction, delta, bulk_TOC1_13C:bulk_TOC2_13C, factor_key=TRUE)
sub_EUP78_d_l <- gather(sub_EUP78_d, fraction, delta, bulk_TOC1_13C:bulk_TOC2_13C, factor_key=TRUE)
sub_EUP910_d_l <- gather(sub_EUP910_d, fraction, delta, bulk_TOC1_13C:bulk_TOC2_13C, factor_key=TRUE)

### summary stats ###

#run the functions length, mean, and sd on the value of "change" for each group,
EUP56_d_stat <- dplyr(sub_EUP56_d_l, c("EUP", "depth"), summarise,
  N = length(delta), mean = mean(delta), sd = sd(delta), se = sd / sqrt(N))
EUP78_d_stat <- dplyr(sub_EUP78_d_l, c("EUP", "depth"), summarise,
  N = length(delta), mean = mean(delta), sd = sd(delta), se = sd / sqrt(N))
EUP910_d_stat <- dplyr(sub_EUP910_d_l, c("EUP", "depth"), summarise,
  N = length(delta), mean = mean(delta), sd = sd(delta), se = sd / sqrt(N))

#plot means plus sd
b_EUP56_delta <- ggplot(EUP56_d_stat, aes(x = mean, y = reorder(depth, desc(depth)))) +
  geom_point(aes(shape = EUP), size = 3, alpha = .5) + geom_path(aes(group = EUP)) +
  scale_shape_manual(values=c(0, 15),
    labels = c("F1 (xantic ferralic Lixisol)", "F2 (ferric Lixisol)")) +
  geom_errorbarh(height=.1, aes(xmin = mean-se, xmax = mean+se)) +
  xlab(expression(dj ^{13}C [\u2030])) + theme_classic() +
  theme(legend.title=element_blank(), axis.text.y=element_blank()) +
  scale_x_continuous(position="top", limits = c(-35,-20), breaks = seq(-35,-20,3))

##### plot same for other depth intervals #####

### plot ###

combined_56 <- b_EUP56_TOC + b_EUP56_delta &
  theme(legend.position = "bottom", legend.justification = "left",
    axis.title.y = element_blank())
combined_56 <- combined_56 + plot_layout(guides = "collect")
combined_78 <- b_EUP78_TOC + b_EUP78_delta &
  theme(legend.position = "bottom", legend.justification = "left",
    axis.title = element_blank(), axis.text.x=element_blank())
combined_78 <- combined_78 + plot_layout(guides = "collect")
combined_910 <- b_EUP910_TOC + b_EUP910_delta &
  theme(legend.position = "bottom", legend.justification = "left",
    axis.title = element_blank(), axis.text.x=element_blank())
combined_910 <- combined_910 + plot_layout(guides = "collect")

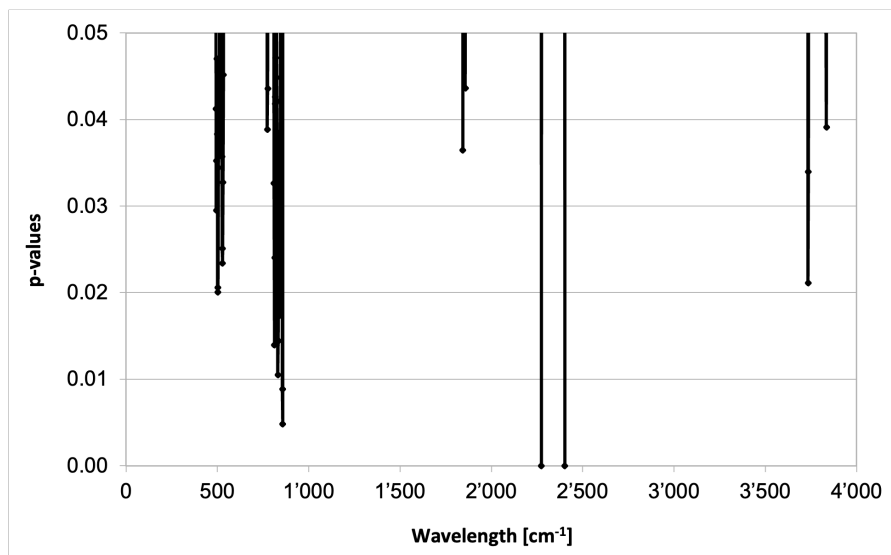
combined_all <- combined_56/combined_78/combined_910
combined_b <- combined_all + plot_layout(guides = "keep")

### export pdf ###
pdf('TOC_bulk.pdf', encoding="MacRoman", height = 8, width = 6)
combined_b
dev.off()
```

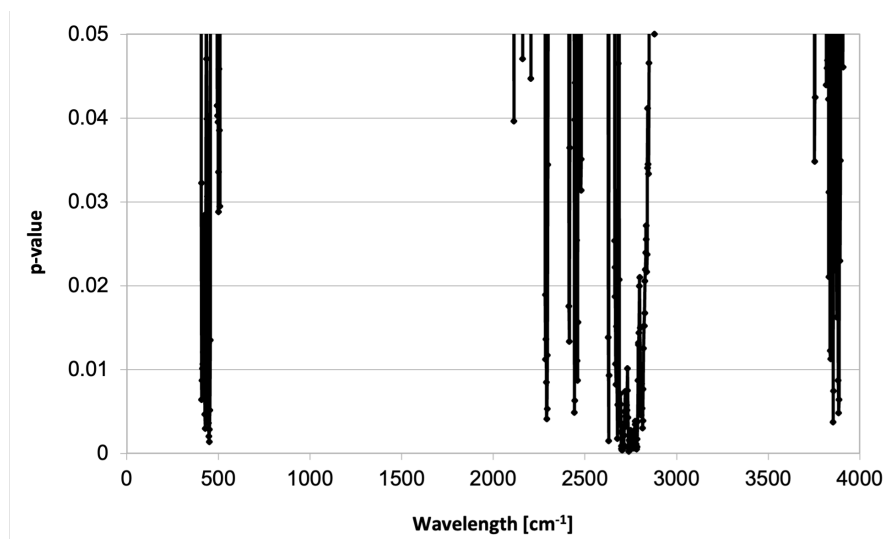
**Figure 22:** Code used to plot the TOC content and  $\delta^{13}\text{C}$  signals. Only the code for bulk soil is shown. However, all other fractions were computed in the same way.

#### A.2.4 DRIFTS: Extraction of integrated band areas and testing the new sample holder

The R code used to extract the integrated band areas of the DRIFT spectra was generously provided by M. Schiedung (marcus.schiedung@geo.uzh.ch). Further, the plotting of compounds ratios was done in the same manner as for the TOC content and  $\delta^{13}\text{C}$  measurements. Moreover, the new, small sample holder used for the measurement of the POM fraction was built by Thomas Keller (UZH). The new holders were compared using a one-sided paired t-test ( $n = 10$  per group) and results are presented in Figure 23.



(a) Distribution of p-values under 0.05 of the t-test between new and standard DRIFTS sample holder for miscanthus.



(b) Distribution of p-values under 0.05 of the t-test between new and standard DRIFTS sample holder for chernozem.

**Figure 23:** The p-values  $< 0.05$  indicate significant differences between the standard and new DRIFTS sample holder.

### A.2.5 Testing correlation variables for normality

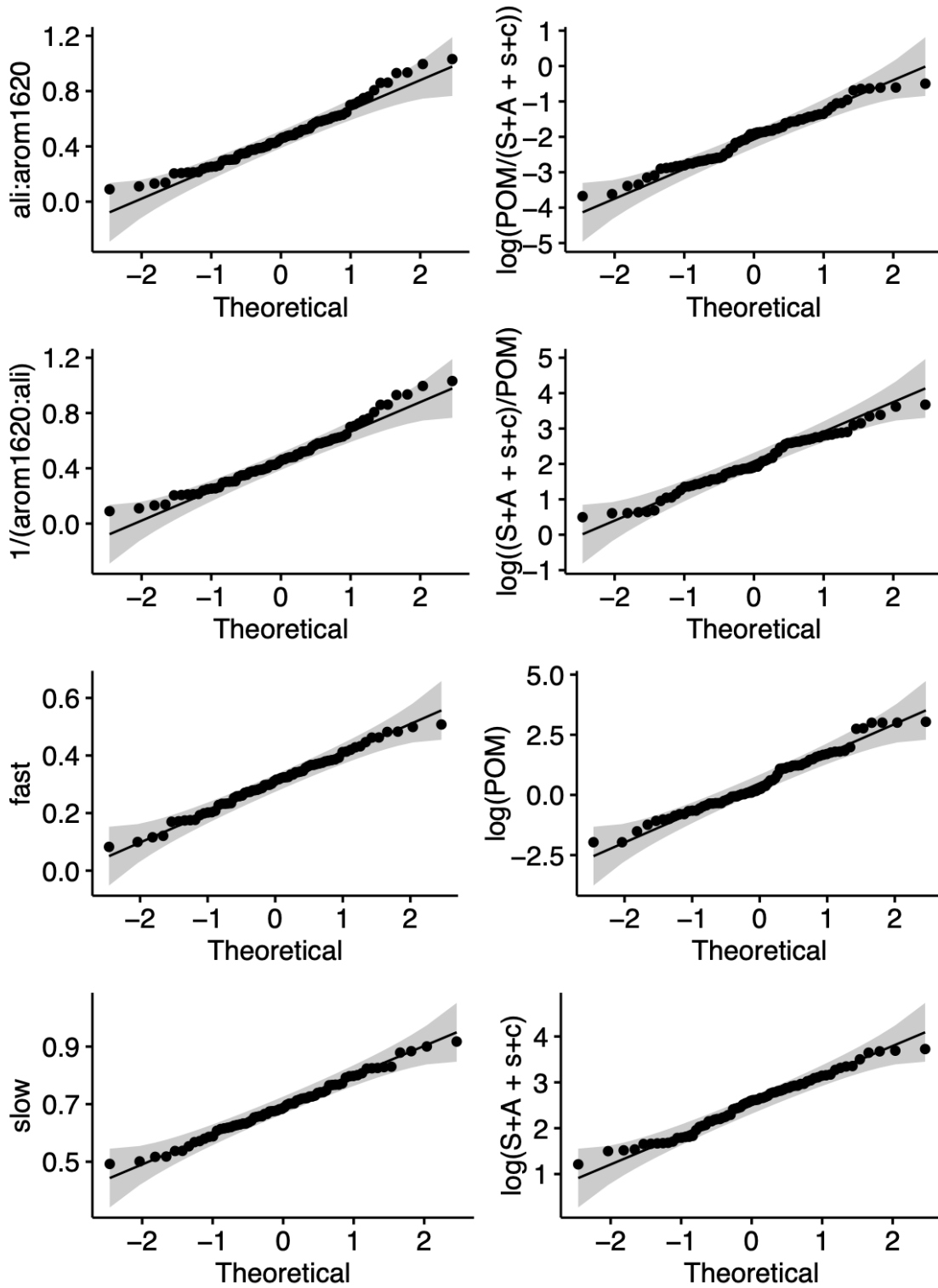


**Figure 24:** QQ-plots of the data used for correlation in section 5.4. Some data was log- or 1/x transformed to fit the assumptions of normal distribution.



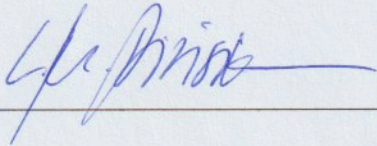
## Personal declaration

I hereby declare that the submitted thesis is the result of my own, independent work. All external sources are explicitly acknowledged in the thesis.

Wiesendangen, 31<sup>st</sup> January 2022

---

Location, Date



---

Lisa Maria Pirisinu